EFFECTS OF IRON LIMITATION AND CARBON SOURCE ON EXTRACELLULAR EXCRETIONS AND INTRACELLULAR CARBON METABOLISM IN PSEUDOMONAS PUTIDA

A Thesis
Presented to the Faculty of the Graduate School
of Cornell University
In Partial Fulfillment of the Requirements for the Degree of
Master of Science

by
Samantha Sarah Sasnow
January 2015

ABSTRACT

Iron (Fe) is an important micronutrient in soils, essential for bacterial growth and carbon metabolism, serving as an enzymatic cofactor for many central carbon metabolic reactions. It has limited bioavailability due to being embedded in Fe oxide and hydroxide minerals. Bacteria secrete high-affinity metal-binding molecules, or siderophores, along with low-affinity organic acids to cope with Fe limitation and facilitate mineral dissolution. In the research presented, I investigated the role of available carbon sources (glucose, succinate, acetate, and citrate) on the secretion of these molecules from the ubiquitous soil bacteria *Pseudomonas putida* and their effectiveness in dissolving Fe from common soil minerals. Fe limited cells secreted the siderophore pyoverdine in addition to secreting higher levels of small organic acids. Dissolution experiments were carried out with bacterial secretions, substrates, and detected organic acids to determine the amount of Fe released with each organic compound. Overall, bacterial secretions were more effective in dissolving Fe than the individual substrates and organic acids. Additionally, to elucidate the changes in metabolic flux with respect to Fe, kinetic and steady-state isotopic labeling experiments were performed with [U-^{13}C] and [1,2-^{13}C] glucose under Fe-limited and replete conditions. Steady-state experiments were also performed with [2,3-^{13}C] succinate under Fe-replete conditions to compare changes in metabolic flux between carbon sources. Overall, most fluxes decreased under Fe-limited conditions with glucose as the sole carbon source, but the flux to the amino acid precursor phosphoenolpyruvate increased. The succinate flux model showed a decrease in flux through the citric acid cycle under Fe-replete conditions, with a corresponding decrease in the amount of CO_2 produced compared to Fe-replete glucose. These findings indicate that the secretion of organic molecules is substrate and Fe dependent, as are the carbon fluxes through the pathways of the central carbon metabolism.

BIOGRAPHICAL SKETCH

Samantha Sasnow earned her Bachelor of Science degrees in Chemistry and Environmental Science from DePaul University in 2012. In 2012, she joined the Biological and Environmental Engineering graduate program at Cornell University. Samantha's thesis research was supervised by Dr. Ludmilla Aristilde, PI. In addition, Dr. Larry P. Walker served on her M.S. thesis committee.

ACKNOWLEDGMENTS

I would like to express my deep appreciation and gratitude to my advisor, Dr. Ludmilla Aristilde, for the mentorship and thoughtful guidance she has provided these past two years. I am also grateful to my other committee member, Dr. Larry P. Walker, for his friendly guidance and kind words. Additionally, I would like to sincerely thank Hua Wei for sharing his knowledge of LC-MS and troubleshooting problems these past two years. Thanks to my fellow lab mates, David Flannelly and Amy Pochodylo, for their help and general support, and finally thanks to Rachel Whiteheart and Sho Yoshitake for being two incredibly hard working undergraduate researchers.

TABLE OF CONTENTS

LIST OF FIGURES

LIST OF TABLES

LIST OF ABBREVIATIONS

Fe	Iron
G6P	Glucose-6-phosphate
F6P	Fructose-6-phosphate
FBP	Fructose-1,6-bisphosphate
DHAP	Dihydroxyacetone phosphate
GAP	Glyceraldehyde-3-phosphate
1,3-bisPG	1,3-bisphosphoglycerate
3PG	3-phosphoglycerate
PEP	Phosphoenolpyruvate
Pyr	Pyruvate
AcCoA, acetyl-CoA	Acetyl coenzyme A
KDPG	2-keto-3-deoxy-6-phosphogluconate
SBP	Sedoheptulose-1,7-bisphosphate
S7P	Sedoheptulose-7-phosphate
R5P	Ribose-5-phosphate
Ru5P	Ribulose-5-phosphate
O8P	Octulose-8-phosphate
OBP	Octulose-1,8-phosphate
E4P	Erythrose-4-phosphate
OAA	Oxaloacetate
2KG	2-ketoglutarate
His	Histidine
Ser	Serine
Gly	Glycine
Cys	Cysteine
Trp	Tryptophan
Tyr	Tyrosine
Phe	Phenylalanine
Val	Valine
Ala	Alanine
Leu	Leucine
Asp	Aspartate
Asn	Asparagine
Thr	Threonine
Lys	Lysine
Met	Methionine
Ile	Isoleucine
Glu	Glutamate
Gln	Glutamine
Pro	Proline
Orn	Ornithine
Arg	Arginine

CHAPTER 1

INTRODUCTION

Iron (Fe) is a limiting micronutrient in soils due to its low solubility in Fe bearing minerals. To facilitate acquisition of Fe, aerobic soil bacteria, as well as many fungi and plants, produce Fe-chelating compounds, or siderophores, in addition to low-affinity organic acids. Different genera of bacteria produce a variety of structurally unique siderophores. *Pseudomonas* secrete the siderophore pyoverdine, among others, under Fe-limited conditions. Siderophore biosynthesis requires energy and rerouting of carbon from biomass production. The present research aims to elucidate the difference in central carbon metabolic flux and secretions of organic acids in *Pseudomonas putida* under Fe-replete and Fe-limited conditions, and to determine the extent to which these organic ligands acquire metal from minerals.

Background

Fe is an essential micronutrient for all living systems (Lim, 2012). Though Fe is abundant throughout soils, its bioavailability is low as it is embedded in Fe oxide and hydroxide minerals of low solubility (Lindsay, 1982). To cope with the scarcity of bioavailable Fe, bacteria have evolved ways to scavenge Fe through the secretion of high-affinity Fe-chelating molecules, or siderophores (Andrews, 2003). High specificity for Fe over other metals facilitates selective acquisition of Fe (Kraemer, 2006). Siderophores mediate Fe acquisition via a two-part process. First, the siderophores chelate Fe in Fe-bearing minerals, thereby inducing mineral dissolution and Fe release (Kraemer, 2006). Second, the Fe-siderophore complex is taken up by the bacteria, the rate of which can be measured using labeled Fe (Royt, 1990). It has been observed that, in

many instances, siderophores can only be taken up by the uptake system of the bacteria that produced them (Lim, 2012). This confers a competitive advantage for capturing the Fe chelated by the corresponding siderophores.

Many bacteria produce siderophores including species of *Pseudomonas*, *Streptomyces* and *Azotobacter* (Hider, 2010). *Pseudomonas* produce a fluorescent yellow-green siderophore, pyoverdine. A relationship between pyoverdine biosynthesis and Fe-limitation was determined decades ago (Meyers, 1978). The exact structure of pyoverdine varies between *Pseudomonas* species, but they are all characterized by three parts: a dihydroxyquinoline chromophore, an acyl group branched from the amino group of the chromophore, and a variable peptide chain that links the carboxyl group of the chromophore with the N-terminus of the peptide chain (Meyer, 2000; Visca, 2010; Figure 1). The chromophoric group, formed from the amino acid tyrosine (Stintzi, 1996), gives the molecule its fluorescence and characteristic yellow-green color in solution. The acyl group can be either an amide or a dicarboxylic acid (Visca, 2007). The length (6 to 12 amino acids) and composition of the peptide chain varies between strains, giving rise to many possible pyoverdine structures, with over 100 configurations identified (Schalk, 2008). However, the binding of Fe is similar among different pyoverdines: Fe(III) is complexed to the chromophore and peptide chain via bonding with oxygen from carboxyl and hydroxyl groups (Meyer, 2000). A multi-transport system, regulated via a cascade of gene signaling, mediates the uptake of Fe-chelated pyoverdine (Schalk, 2007). An outer membrane transporter binds to pyoverdine and transfers it to the perisplasm, wherein Fe dissociates from pyoverdine, is reduced and subsequently bound to a periplasmic protein. A second transporter on the inner membrane then transfers the Fe into the cytoplasm (Schalk, 2007).

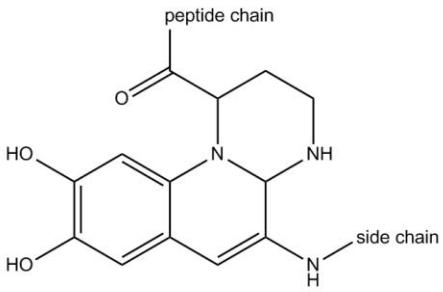

Figure 1. Pyoverdine structure

Pseudomonads are known to secrete organic acids in addition to siderophores that are important in metal acquisition and cycling. An abundance of glucose as the carbon source led to secretions of large amounts of 2-ketoglutarate (Koepsell, 1952) and pyruvate (Asai, 1955) in a strain of *Pseudomonas fluorescens*. Gluconate, oxalate, succinate, citrate and malate were secreted by *Pseudomonas* in order to solubilize inorganic phosphate (Vyas, 2009). These organic ligands are capable of facilitating mineral dissolution and biological uptake of metals in addition to Fe, including Mn (Duckworth, 2005), Co (Bi, 2010), Al (Evers, 1989) and Cu (Hemlem, 1996), which contributes to the plant growth promoting capabilities of Pseudomonads. In particular, citrate facilitates Cu and Fe dissolution in chalcopyrite (Goyne, 2006) and Fe dissolution in goethite, a common Fe-bearing mineral (Reichard, 2007; Cheah, 2003). Succinate and fumarate also enhance dissolution of goethite in solution with siderophore (Reichard, 2007; Cheah, 2003).

Pseudomonas putida is a ubiquitous aerobic soil bacterium noted for its metabolic diversity that has been extensively studied for environmental bioremediation and for human and environmental health concerns (Poblete-Castro, 2012). It is amongst the rhizobacteria found near plant roots and plays an important role in plant-bacteria symbiosis (Molina, 2000); it grows on

plant root exudates and, through siderophores and organic ligands secretions, increases the availability of metals. *P. putida* is capable of degrading a wide variety of organic contaminants (Poblete-Castro, 2012; Mansour, 2012; Mansour, 2012) and has been studied for its use in bioremediation of various contaminants, including pharmaceuticals and aromatics (Mansour, 2012; Hinteregger, 1992), and its use in wastewater treatment facilities (Nigam, 2012). *P. putida* has been exploited for biotechnological applications and synthesis of polymer precursors (Poblete-Castro, 2012). The carbon metabolism of *P. putida* has been well studied, but the effect of different environmental stressors on carbon metabolism remains unclear. As mentioned previously, pyoverdine biosynthesis under Fe-limited conditions requires several amino acid biosynthetic pathways. The research for this project is based on the hypothesis that *P. putida* will reroute central carbon metabolism to favor biosynthesis of metabolic precursors to amino acids when grown on different carbon substrates under Fe-limited conditions. Additionally, *P. putida* will produce a different array of low-affinity organic ligands under these growth conditions that will aid in mineral dissolution and metal uptake. Elucidating the changes in metabolic flux under Fe-limited conditions will provide a better understanding of *P. putida* and broaden its use in environmental engineering and biotechnological applications.

Genomics, proteomics, and most recently, metabolomics have been applied to study the metabolism of *P. putida* (van der Werf, 2008; Sudarsan, 2014; Blank, 2008). *P. putida* is noted for lacking the gene that codes for 6-phosphofructokinase, which is responsible for converting fructose-6-phosphate to fructose-1,6-bisphosphate. Thus, the Embden-Meyerhof-Parnas (EMP) pathway is not fully functional in Pseudomonads (Poblete-Castro, 2012). Consequently, glucose is metabolized primarily via the Entner-Doudoroff (ED) pathway (Castillo, 2007; Wang, 1959; Wood, 1954; Figure 2A). Once glucose is taken up by *P. putida*, it is either oxidized to gluconate

or phosphorylated to glucose-6-phosphate, both of which can be converted to 6-phosphogluconate, an important intermediate that feeds both the ED pathway (Poblete-Castro, 2012) and the oxidative PP pathway (Blank, 2008; Figure 2A and 2B). The ED pathway feeds into lower glycolysis via the formation of pyruvate and glyceraldehyde-3-phosphate. Lower glycolysis eventually routes pyruvate to the tricarboxylic acid (TCA) cycle, which provides metabolite precursors to several amino acid biosynthetic pathways (Figure 3). In the TCA cycle, the glyoxylate shunt is also present in *P. putida* (Ebert, 2011), converting citrate to succinate and glyoxylate, which then combines with acetyl-CoA to form malate (Figure 3). The pentose phosphate (PP) pathway is also active, yielding DNA and RNA precursors (Figure 2B).

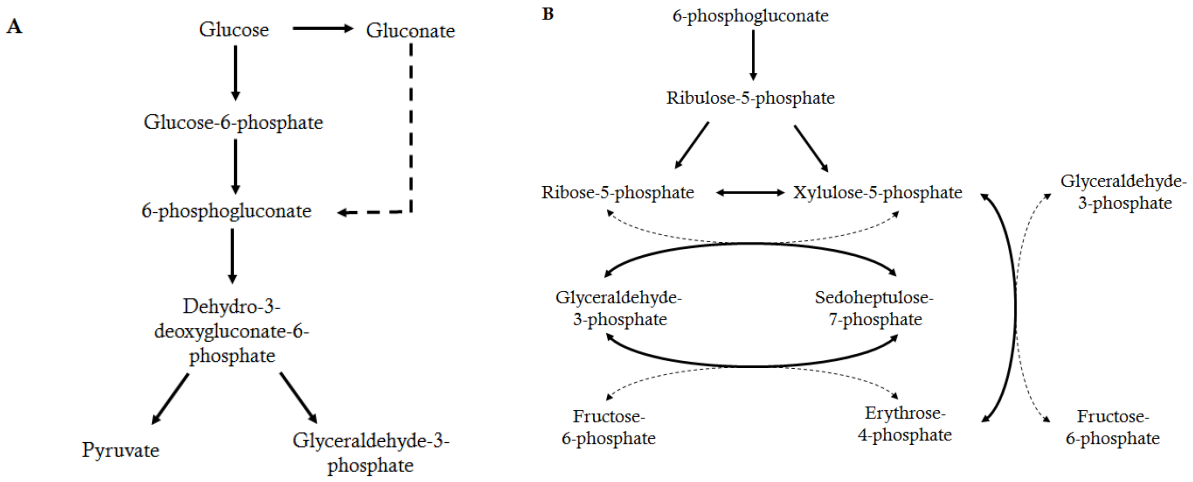

Figure 2. (A) Entner-Doudoroff pathway and (B) pentose-phosphate pathway

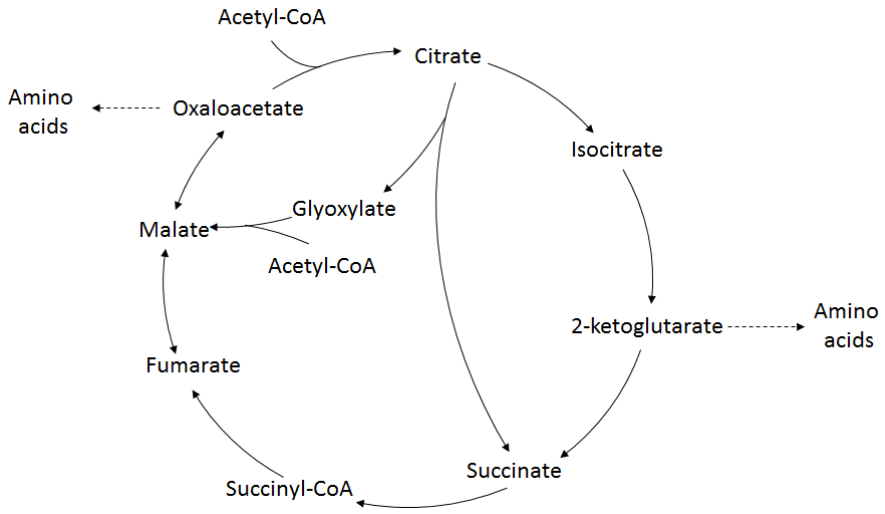

Figure 3. Glyoxylate shunt in the TCA cycle

The effects of Fe on the overall metabolism of microorganisms have been well studied (Shakoury-Elizeh, 2010; Folsom, 2014; Filiatraut, 2010). However, the effect of carbon source assimilation on metabolism under different Fe conditions in *Pseudomona*s has not been well studied. A previous study with *Saccharomyces cerevisiae* looking at the effects of Fe deficiency attributed the disruption in glucose metabolism, along with lipid and amino acid biosynthesis, to the loss of Fe cofactors in enzymes with Fe-S clusters (Shakoury-Elizeh, 2010). Under Fe-limited conditions, the genes in *S. cerevisiae* involved in the cellular respiration process were down regulated resulting in lower levels of glycolytic intermediates and increased levels of pyruvate, favoring fermentation (Shakoury-Elizeh, 2010; Philpott, 2012). Fe limitation has been shown to affect membrane lipid composition in algae (Urzica, 2013), to control the regulation of virulence genes in the pathogenic bacterium *Pseudomonas syringae* (Kim, 2009), and to reduce the degradation of polycyclic aromatic hydrocarbons in *Pseudomonas citronellolis* and *Pseudomonas aeruginosa*, presumably by reducing the activity enzymes responsible for aromatic

compound metabolism (Santos, 2007). Additionally, when toluene is the sole carbon source, toluene degradation in *P. putida* decreases under Fe limiting conditions due to a reduction in toluene-degrading enzymes (Dinkla, 2002). In sum, these studies show that Fe levels can control the regulation of genes and enzymes involved in metabolic processes, but the changes in flux of the corresponding metabolic pathways remain to be elucidated.

Metabolic flux analysis (MFA) is a mathematical approach which combines experimental results with computer modeling to provide a quantitative understanding of the systems-level metabolism in microorganisms. MFA is thus a useful tool in metabolic engineering to determine how the metabolic network of organisms responds to environmental stresses and to reveal if any pathways are favored, a necessary step when using *P. putida* and other bacteria in bioremediation and other biotechnological applications. Specifically, MFA is used to estimate fluxes in different biosynthetic pathways. Stable isotopes (^{13}C typically) are used to track assimilation of labeled carbon substrates whereby metabolic pathways produce distinct isotopic patterns of metabolite labeling depending on the metabolic flux of the labeled substrate (Zamboni, 2009). Samples are taken at steady-state (Yuan, 2008) or from kinetic (Amador-Noguez, 2010) isotopic experiments, measured for metabolite abundances and then used in a computer model to determine fluxes. A complete stoichiometric reaction network and a mass balance on carbon are needed to accurately predict metabolic fluxes via computer modeling. In the past, gas chromatography-mass spectrometry (GC-MS) was typically used to analyze labeling abundance in metabolites due to its ability to detect a number of intracellular metabolites, especially amino acids and other biomass precursors, with high accuracy (Blank, 2008; del Castillo, 2007; Fuhrer, 2005). Accordingly, the labeling patterns of central carbon metabolites were primarily inferred from amino acid labeling. Liquid chromatography-mass spectrometry (LC-MS) can measure

metabolites without the need for derivitization of non-volatile compounds, offering a greater range of measurable metabolites and better detection capabilities (Wenyun, 2010). Different modeling programs are used to conduct system-wide MFA, the program 13CFLUX2 is used in the present study. 13CFLUX2 uses stoichiometric equations and mass isotopomer data, which provides the number of labeled carbons present in each metabolite, to estimate intracellular fluxes (Yuan, 2008; Weitzel, 2013).

The present research will build on previous studies of *P. putida* metabolism to investigate the response of central carbon metabolic pathways to Fe while also elucidating to what extent the siderophore pyoverdine and small organic acids facilitate metal release from mineral dissolution. *P. putida* has been shown to produce pyoverdine under Fe-limited conditions but no studies have been conducted to understand how metabolism is rerouted to meet the expensive carbon budget required for pyoverdine biosynthesis. This research will provide a more mechanistic understanding of the role of environmental stresses on carbon metabolism and organic carbon cycling, which will ultimately lead to a better elucidation of the importance of rhizobacteria in plant matter respiration and CO_2 emissions. Determining how the metabolism of *P. putida* reacts in response to changing environmental conditions is also essential to improving its use in bioengineering and biotechnology.

CHAPTER 2

METHODS

Organic acid secretions

P. putida KT2440 was obtained from ATCC and plated on solid agar Luri-Bertani (LB) medium, stored at 4 °C. Individual colonies were selected from solid agar plates and cultured in liquid LB medium to saturation prior to transfer to minimal media containing different organic substrates. Liquid culturing was performed in 20-mL glass test tubes or 250-mL Erlenmeyer flasks in an incubator set to 20 °C on an orbital shaker at 200 rpm (1 in orbit). The tubes and flasks were capped with sponge caps to limit contamination and allow proper air circulation. Bacteria were grown in pH-adjusted (7.0) and filter sterilized minimal growth media containing the following salts: 20 mM KH_2PO_4, 5 mM NaH_2PO_4, 0.8 mM $MgSO_4 \cdot 7H_2O$, 37 mM NH_4Cl, 34 µM $CaCl_2 \cdot 2H_2O$, 13 µM $CuSO_4 \cdot 5H_2O$, 0.97 µM H_3BO_3, 70µM $ZnSO_4 \cdot 5H_2O$, 5.9 µM $MnSO_4 \cdot 5H_2O$, 0.21 µM $NiCl_2 \cdot 5H_2O$, 1.2 µM $Na_2MoO_4 \cdot 5H_2O$ and 308 mM of carbon source (glucose, succinate, citrate or acetate). Bacteria were grown on Fe-replete and Fe-limited conditions. Fe-replete conditions consisted of minimal media with 20 µM of added Fe in the form of $FeSO_4$ $7H_2O$. Fe-limited conditions consisted of minimal media with no added Fe. Growth was monitored by measuring the optical density (OD_{600}) of bacteria cells with an Agilent Cary UV-visible spectrophotometer. The initial OD_{600} of the cells in the first transfer of minimal media was between 0.05 and 0.07. First bacterial transfer consisted of aliquots of saturated LB media transferred to minimal media with carbon source and with or without Fe. When the cell growth of the first transfer tubes reached late exponential phase, bacteria were transferred again to fresh media. This guaranteed *P. putida* was fully adapted on the specific carbon source.

Samples for extracellular excretions were taken at the onset of early stationary growth phase. Samples (1-mL) were centrifuged (21,130*g* for 5 min) and filtered (0.22 µm nylon filters) to remove cells. Samples were diluted (1:10 or 1:100) in LC-MS grade water, to prevent oversaturation of metabolites, and spiked with benzoate as an internal standard. Metabolites were analyzed by reversed-phase ion-pairing liquid chromatography (Thermo) coupled with electrospray ionization (ESI) mass spectrometer (Q Exactive) operated in full scan negative mode (*m/z* range 70 to 900) for the detection of metabolites based on accurate masses. A Synergy Hydro-RP column (100 mm x 2 mm and 2.5 µm particle size, Phenomenex) was used. Solvent A contained 97:3 (v/v) water/methanol with acetic acid (15 mM) and tributylamine (10 mM), which served as an ion-pairing reagent to enhance LC retention of metabolites. Solvent B was 100% methanol. The flow rate was 200 µL/min with a solvent B gradient of 0%; 2.5 min, 0%; 5 min, 20%; 7.5 min, 20%; 10 min, 55%; 12 min, 55%; 14 min, 95%; 17 min, 95%; 18 min, 0%; 25 min, 0%. The sample injection volume was 10 µL and the column temperature was set to 25 °C. The Maven software package was used to process data. Metabolites were quantified using individual standards at known concentrations. The following metabolites were quantified extracellularly: citrate, gluconate, succinate, pyruvate, hydroxybenzoate, 2-ketoglutarate, glutamate, fumarate, aspartate and malate. Organic acids were OD normalized before comparison.

Mineral dissolution

Experiments were carried out in 50-mL polypropylene tubes that were washed with HNO_3 (15% v/v) twice to remove residual trace metals and sterilized in an autoclave to prevent bacterial growth during the experiments. Mineral dissolution solutions contained Fe-minerals (1g/L),

goethite, magnetite or hematite in 10-mL of solution. Experiments were conducted with extracts from stationary growth phase of Fe-limited *P. putdia* on citrate, succinate, glucose or acetate grown in 250-mL Erlenmeyer flasks in an incubator shaker (New Brunswick I24R) set to 200 rpm (1 in orbit) and 20°C. Extracts were centrifuged (21,130*g* for 5 min) and filtered (0.22 µm nylon filters) to remove cells. Solutions were then pH-adjusted (7.5) and filter sterilized. Control experiments consisted of minimal media with each carbon source (100 mM: glucose, succinate, citrate or acetate) and no added Fe, minimal media with detected secreted acids (gluconate, pyruvate, citrate, 2-ketoglutarate, glutamate, succinate, fumarate, malate, or aspartate: 10 mM), or pyoverdine standard (100 µM). The pyoverdine standard was obtained from Sigma Aldrich and was isolated from a *Pseudomonas fluorescens* strain. Blanks were also performed for minerals in minimal media and each carbon source in minimal media without the presence of minerals. Sample vessels were wrapped in aluminum foil to prevent photochemistry and placed in an incubator shaker set at 20°C and 200 rpm. Samples (6-mL) were taken after 100 hr, centrifuged and filtered to remove minerals. Before storage and analysis, samples were pH-adjusted to 4.5 using an acetate buffer to prevent bacterial growth and dissolve all Fe. Total Fe was measured via inductively coupled plasma atomic emission spectroscopy (ICP-AES, Spectro Analytical) analysis (detection limit = 36 nM). Fe concentrations were then blank corrected with corresponding blanks. Samples from the extracts were also used to quantify pyoverdine in each solution. Pyoverdine was quantified by adjusting the supernatant to 7.0 using KOH (2M) for acidic solutions (glucose) and HCl (1M) for basic solutions (succinate, acetate, citrate). Because pyoverdine concentrations were high, samples were diluted (from 1:20 to 1:100) in minimal media. Fluorescence was then measured at excitation and emission wavelengths of 403 and 463

nm, respectively, using an Agilent Cary Eclipse fluorescence spectrophotometer. Pyoverdine was quantified using a *P. fluorescens* standard (Sigma Aldrich) to create a standard curve.

Kinetic isotopic labeling

Batch cultures were grown in minimal media containing unlabeled glucose (308 µM of C; with added Fe or no added Fe) until an early exponential OD_{600} of 0.2 to 0.35 was reached. Aliquots of 3-mL were filtered through nylon filters and transferred to solid agar minimal media plates with glucose (308 µM of C). Growth was measured by washing parallel cultured plates with 3-mL of growth media and measuring OD_{600}. Samples were grown to allow for multiple doubling times before harvesting. Once an optimal OD was reached (0.8-1.0), filters with bacteria were then transferred to minimal media plates containing either [U-^{13}C] glucose or [1,2-^{13}C] glucose as the sole carbon source. At increment time points after the initial transfer (0s, 30s, 1 min, 2min, 5 min, 15 min, 30 min, 60 min), metabolism was quenched using a 40:40:20 solvent mixture and extracts were prepared and analyzed as mentioned above. The isotopomers of ^{13}C labeling were measured using LC-MS and analyzed with the Maven software suite.

Steady-state isotopic labeling

Bacteria were cultured in 20-mL test tubes in an incubator set to 30 °C on an orbital shaker at 200 rpm (1 in orbit) with minimal media containing unlabeled glucose (with or without added Fe) or succinate (with added Fe) until mid-exponential phase. Bacteria were then transferred to 20-mL tubes with minimal media with or without added Fe and either [1,2-^{13}C] glucose or [2,3-^{13}C] succinate as the sole carbon source. Bacteria were grown until an OD_{600} of 0.6-0.8 was reached. These ODs fell within the exponential growth phase of each condition and were taken

as pseudo steady-state condition. Aliquots of 2-mL were taken and filtered through 0.22 nylon filters. Samples were immediately quenched with a solution (2-mL, 4 °C) of methanol, acetonitrile and water (40:40:20, respectively). Cell mass was washed off the filters using a pipette. The solution was then vortexed, centrifuged (21,130*g* for 5 min at 4 °C), and filtered to remove lysed cells. 200 µL of sample were then transferred to LC-MS vials and analyzed for isotopic labeling of intracellular metabolites with the same method mentioned above.

Intracellular metabolite quantification

To compare metabolite pools between Fe conditions, intracellular metabolites were quantified using [U-^{13}C] glucose. Bacteria were first cultured in minimal media with or without Fe and [U-^{13}C] glucose as the sole carbon source (30°C, 200 rpm shaker). At late exponential phase, bacteria were transferred to fresh medium with the same composition; this was to assure all metabolites were fully labeled with ^{13}C. Bacteria were harvested during early exponential phase (OD_{600} 0.6-0.8). LC-MS samples were prepared with the same method as steady state samples mentioned previously. Before analyzing via LC-MS, samples were spiked with known concentrations of metabolites (20 µM) and the internal standard benzoate (20 µM). Blanks of extracellular media were analyzed to ensure quantified metabolites were intracellular. Intracellular metabolite concentrations were calculated using the ratio of labeled metabolite to the abundance of unlabeled metabolite.

Metabolic flux analysis

To perform metabolic flux analysis on the steady-state data, metabolite excretion and substrate consumption rates were required for a complete mass balance on carbon. Bacteria were cultured

in minimal media with or without added Fe and either glucose or succinate (308 µM of C) as the sole carbon source. Samples (1-mL) were taken during early exponential growth phase for consumption measurements and for extracellular metabolites. Consumption was monitored using high resolution ^{1}H nuclear magnetic resonance (NMR). NMR samples were prepared using 440 µL of cell-solutions, 60 µL D_2O, 50 µL 2,2-dimethyl-2-silapentane-5-sulfonate (DSS) and 50 µL Na-azide. D_2O provided a field-frequency lock, DSS was used as a reference for chemical shift and served as an internal standard, and Na-azide was used to prevent bacterial growth. NMR spectra (relaxation delay of 5 s, recording of 16 scans per sample, receiver gain of 38 dB) were recorded at 25 °C on a Varian Unity INOVA 600-MHz NMR spectrometer. The water signal suppression was obtained by applying the presaturation (preset) pulse sequence. Spectra were phased and baseline corrected using MestReNova (version 8.1.2).

Excretion rate samples were taken during early exponential growth phase corresponding to the OD_{600} of each steady state experiment. Samples were prepared for LC-MS analysis as mentioned above for organic acid secretions. Metabolites were quantified using known concentration of metabolite standards. Excretion rates were calculated (uM/OD) and converted to uM/gCDW/hr by using an OD to biomass conversion factor for *P. putdia* (Van Duuren, 2013). Consumption rates (mM/OD) were converted to uptake rate using the growth constant and biomass conversion factor. Excretion rates were normalized to the uptake rate before use in the model. Biomass conversion rates were calculated for amino acid precursors and the nucleotide precursor ribose-5-phosphate by using reported literature values for amino acids molar ratios (Van Duuren, 2013) and normalizing to the uptake rate. Molar ratios of nucleotides were calculated using the genome of *P. putida* KT2440 (PGD, 2014). To account for pyoverdine biosynthesis under Fe-limited conditions, a value for the conversion of metabolites to pyoverdine

biomass was calculated using the amount of pyoverdine secreted over time when grown on glucose (from mineral dissolution experiments) and converted to a fraction of the uptake rate. This was then added to the precursors to compounds identified in the most abundant pyoverdine produced by *P. putida* when grown on glucose under Fe-limited conditions (work done by Hua Wei, post doc, Aristilde lab). Most of the excretion rates and biomass conversion rates were set as constraints in the model, but some rates were determined as constrained variables. These specific excretion rates or biomass conversion rates were constrained with inequalities, and any excretion rate that fell below 6% of the uptake rate was considered valid. For the glucose (+)Fe and (-)Fe models, aspartate LC-MS labeling data was used in place of oxaloacetate labeling data. As aspartate only forms from oxaloacetate (Figure 4), it was assumed the labeling patterns in aspartate would be consistent with those of oxaloacetate, which was not measurable via LC-MS. Labeling data for 3-phosphoglycerate, phosphoenolpyruvate, pyruvate, citrate, 2-ketoglutarate, fumarate, aspartate and glutamate were used to model the TCA cycle for *P. putida* grown on succinate under Fe-replete conditions. To model *P. putida* grown on glucose under (+)Fe and (-)Fe conditions, additional metabolites were used to model the complete central carbon metabolism: glucose-6-phosphate, fructose-6-phosphate, fructose-1,6-bisphosphate, dihydroxyacetone phosphate, gluconate, 6-phosphogluconate, ribose-5-phosphate, xylulose-5-phosphate, sedoheptulose-7-phosphate, sedoheptulose-1,7-phosphate, succinate, and octulose-8-phosphate.

The software suite 13CFLUX2 was used to perform metabolic flux analysis. This software uses a constructed metabolic network, LC-MS isotopomer labeling data, measured excretion and uptake rates, and stoichiometric constraints to estimate a feasible stoichiometric null space before calculating metabolic reaction rates using custom-made algorithms (Weitzel,

2012). First, a set of initial flux values are determined by the program. Then, fluxes are optimized based on constraints. During optimization, the model estimates labeling patterns based on the calculated fluxes from the stoichiometric network. The quality of fit between experimental and estimated labeling patterns is reported by the model as residuals, and based on these values, the user determines an endpoint for the optimization (Zamboni, 2009). For the metabolic flux analysis presented here, estimated labeling patterns were compared to the LC-MS steady-state labeling patterns for each model to validate the fluxes.

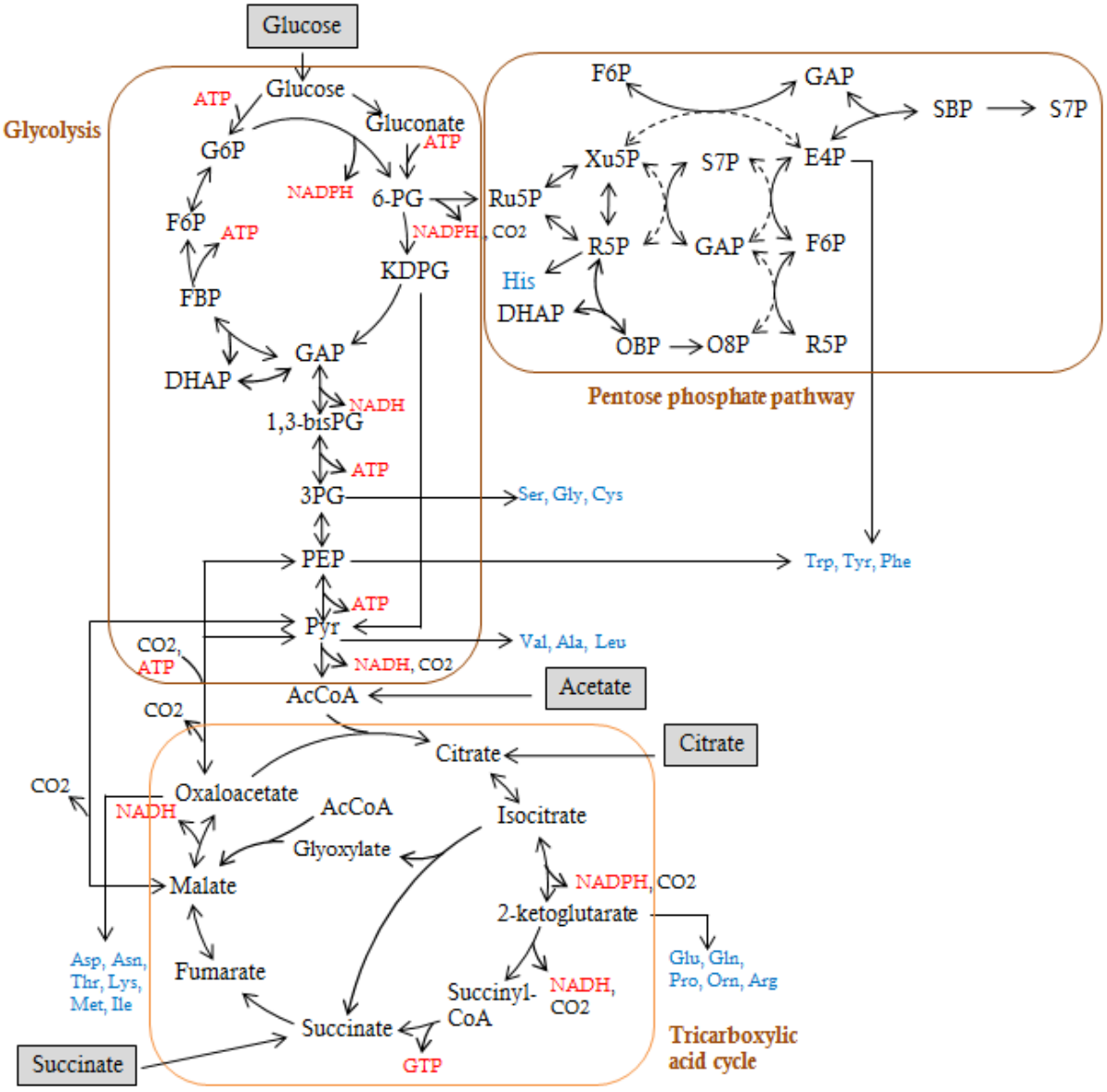

Figure 4. Metabolite map of central carbon metabolism in *P. putida*. Amino acids are highlighted in blue next to their precursor compounds. Compounds in grey boxes represent the point of entry of different carbon substrates (glucose, acetate, citrate, succinate). Abbreviations are as follows: glucose-6-phosphate, G6P; fructose-6-phosphate, F6P; fructose-1,6-phosphate, FBP; dihydroxyacetone phosphate, DHAP; glyceraldehyde-3-phosphate, GAP; 1,3-bisphosphoglycerate, 1,3-bisPG; 3-phosphoglycerate, 3PG; phosphoenolpyruvate, PEP; pyruvate, Pyr; acetyl-coenzyme A, AcCoA; 6-phosphogluconate, 6-PG; ribulose-5-phosphate, Ru5P; xylulose-5-phosphate, X5P; ribose-5-P, R5P; erythrose-4-phosphate, E4P; sedoheptulose-7-phosphate, S7P; sedoheptulose-1,7-phosphate, SBP; octulose-8-phosphate, O8P; octulose-1,8-phosphate, OBP. Metabolite map gathered from multiple sources (Blank, 2008; Sudarsan, 2014; Poblete-Castro, 2012; Fuhrer, 2005; del Castillo, 2007).

CHAPTER 3

EXTRACELLULAR EXCRETIONS AND MINERAL DISSOLUTION

High- and low-affinity extracellular excretions

The fluorescent yellow-green siderophore, pyoverdine, is secreted by *Pseudomonas* bacteria, among other siderophores, under Fe-limited conditions in order to facilitate Fe acquisition (Cornelis, 2010; Meyer, 2000; Ravel, 2003; Visca, 2007). Pyoverdines produced by *Pseudomonas* contain the same dihydroquinoline chromophore and fluorescence signature (Ravel, 2003). Using this fluorescence signature, no detectable amount of pyoverdine was found in the (+)Fe media, but pyoverdine was consistently present in (-)Fe media (Table 1).

Siderophore production by *Pseudomonas* has previously been shown to be carbon source-dependent. Extracellular pyoverdine concentrations varied when *P. syringae* and *P. viridiflava*, both pathogenic bacteria, were grown on different amino acids under Fe-limited conditions (Bultreys, 2000). Pyochelin production, another type of Fe-chelating siderophore produced by some *Pseudomonas*, was shown to vary when *P. fluorescens* was grown on fructose, mannitol, sucrose, glycerol and glucose; the highest amounts of extracellular pyochelin were measured with fructose, mannitol and glucose (Duffy, 1999). These findings suggest that along with limited Fe, carbon source plays a significant role in siderophore production. In the experiments presented, the amount of pyoverdine secreted was substrate dependent (Table 1), with the highest amount of pyoverdine being found in the presence of citrate (405±118 µM) and acetate (145±3 µM), followed by succinate (93±14 µM) and glucose (69±10 µM). The difference in pyoverdine secretion may be a result of different entry points in the metabolic network (Figure 4). Pyoverdine structures have been characterized for different Pseudomonas strains, most notably

the variable peptide backbone has been determined for a number of pyoverdines, ranging from 6 to 12 amino acids in length (Meyer, 2000). Certain amino acids are common throughout these characterized pyoverdines, namely serine, glutamine, ornithine, alanine, aspartate, and threonine. The position of these amino acids in relation to uptake of each substrate explains the variation in pyoverdine excretion. Once citrate is taken up, it is converted to isocitrate and then 2-ketoglutarate, which is the precursor to glutamine and ornithine, two amino acids commonly found in pyoverdine. Although succinate and citrate metabolism begin in the TCA cycle, they must go through gluconeogenesis to reach the PP pathway in order to form nucleotides. Sudarsan et al. looked at the metabolism of benzoate, a compound that metabolizes by first splitting into acetyl-CoA and succinate (Figure 3), and found half of the TCA cycle (from succinate to pyruvate) had a significantly higher flux than the other half (oxaloacetate to succinate), indicating a TCA cycle favoring flux into lower gluconeogenesis (Sudarsan, 2014). Glucose is not the preferred carbon source of *P. putida* (Poblete-Castro, 2010), which may explain why the extracellular media, when grown on glucose, contained the lowest levels of pyoverdine.

Table 1. Pyoverdine concentration in extracellular media at early stationary growth phase

Substrate	*OD at early stationary phase*	*Pyoverdine Concentration(µM) ± Standard Error (n=2)*
Glucose	1.36±0.15	69±10
Citrate	3.66±.020	405±118
Succinate	1.30±0.11	93±14
Acetate	0.95±0.09	145±3

In addition to high-affinity binding ligands, *Pseudomonas* can secrete small organic acids capable of mediating metal acquisition (Vyas, 2009; Trivedi, 2008; Rodriguez, 1999; Illmer, 1992), thus, facilitating metal cycling and promoting plant growth. These small organic acids can promote mineral dissolution (Goyne, 2006; Reichard, 2007; Cheah, 2003) and enhance bioavailability of metals in the presence of high-affinity ligands (Aristilde, 2012). The TCA

cycle includes metabolic reactions which produce several organic acids known to be secreted by rhizobacteria (Goyne, 2006; Reichard, 2007; Cheah, 2003). For instance, *Pseudomonas* have been shown to secrete gluconate, pyruvate, 2-ketogluconate, oxalate, malate, succinate, 2-ketoglutarate and citrate during inorganic phosphate solubilization (Vyas, 2009; Trivedi, 2008; Otto, 2011). 2-ketoglutarate secretion has been observed in other bacteria and yeast (Otto, 2011). To determine the effects of organic substrates and limited Fe on secreted organic acids, ten organic acids present at high levels (>10 nM) were characterized and quantified (citrate, succinate, 2-ketoglutarate, glutamate, fumarate, malate, aspartate, gluconate, pyruvate and hydroxybenzoate) in the extracellular media of *P. putida* grown on citrate, succinate and acetate under Fe-limited and Fe-replete conditions in addition to *P. putida* grown on glucose under Fe-limitation (Figures 5 and 6). Results were compared with the growth of *P. putida* on glucose under Fe-replete condition, which was previously conducted (Hua Wei, postdoc, Aristilde lab).

Overall, Fe-limited media contained higher concentrations of secreted organic acids than Fe-replete media, with the exception of glutamate (Figure 5) and aspartate (Figure 6), which were higher in (+)Fe glucose media. Pyruvate, hydroxybenzoate, citrate, 2-ketoglutarate, and succinate, on average, were higher in (-)Fe media when *P. putida* was grown on citrate, succinate and acetate (Figure 5, Figure 6 and Table 2). Overall citrate, 2-ketoglutarate, glutamate and pyruvate had the highest average secretions across both Fe conditions (Figure 5). The high concentrations of these organic acids may be due to overflow metabolism, a mechanism that occurs when feedback inhibition is ineffective and results from an imbalance between substrate uptake fluxes and those for energy production and biomass growth (Cornish-Bowden, 2013; Reaves, 2013). Metabolite concentrations can thus be regulated by demand, degradation, and excretion (Cornish-Bowden, 2013). To conserve energy when carbon influx is high, bacteria

excrete metabolites instead of assimilating them into the metabolic network. This phenomenon has been reported in *E. coli* and yeasts (Han, 1992; Vemuri, 2006; Vemuri, 2007), which excrete growth-inhibiting side products like acetate and ethanol.

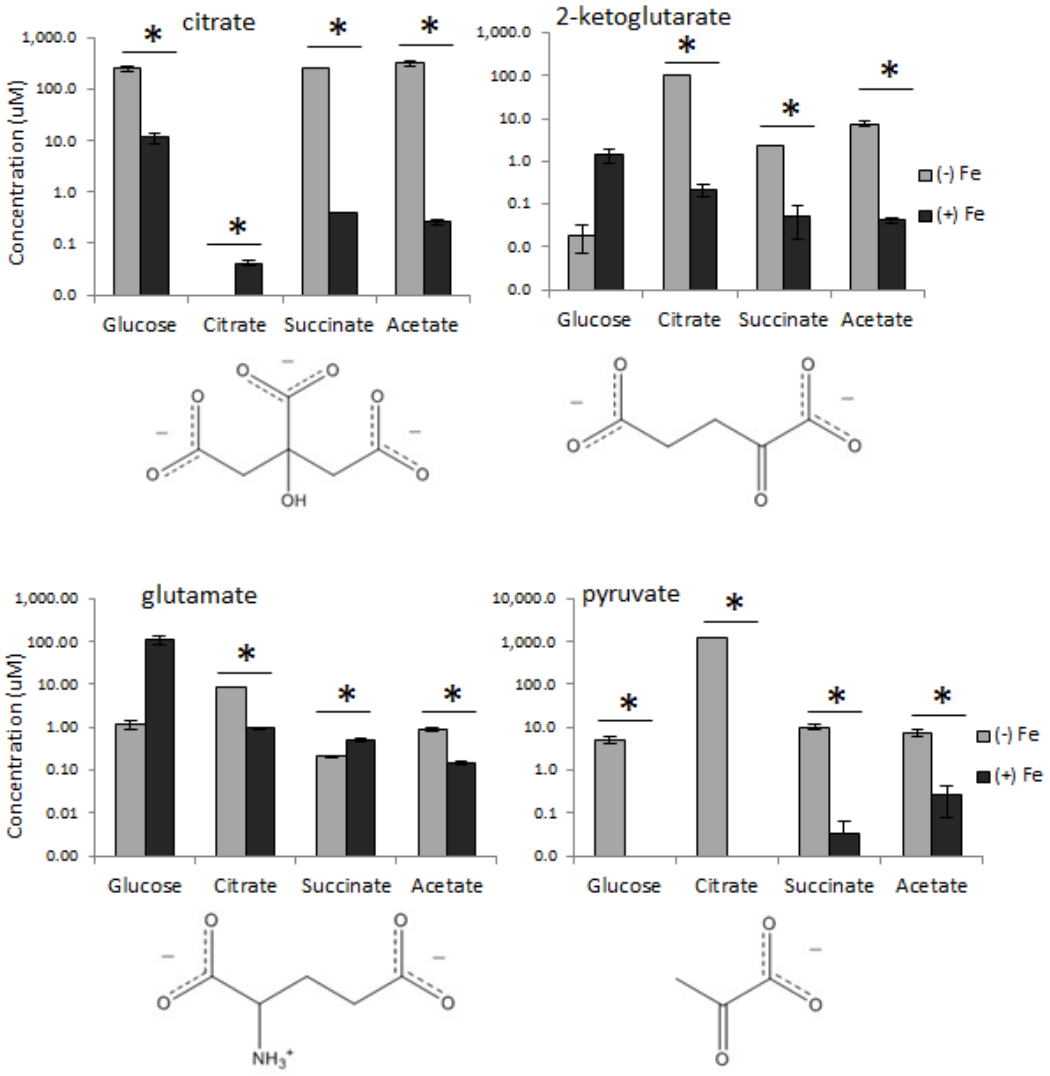

Figure 5. Concentration (µmol L^{-1}) of excreted organic acids (with highest abundance) in the early stationary phase of growth on each substrate (glucose, citrate, succinate and acetate) under Fe-replete (black bars) and Fe-limited (grey bars) conditions. Data shown are mean values ± standard error (n=2). Glucose (+)Fe data was performed by Hua Wei (post doc, Aristilde lab) and are used as a comparison to other carbon substrates and glucose (-)Fe data. Asterisks (*) indicate a statistically significant (p value < 0.05) difference between the two Fe conditions.

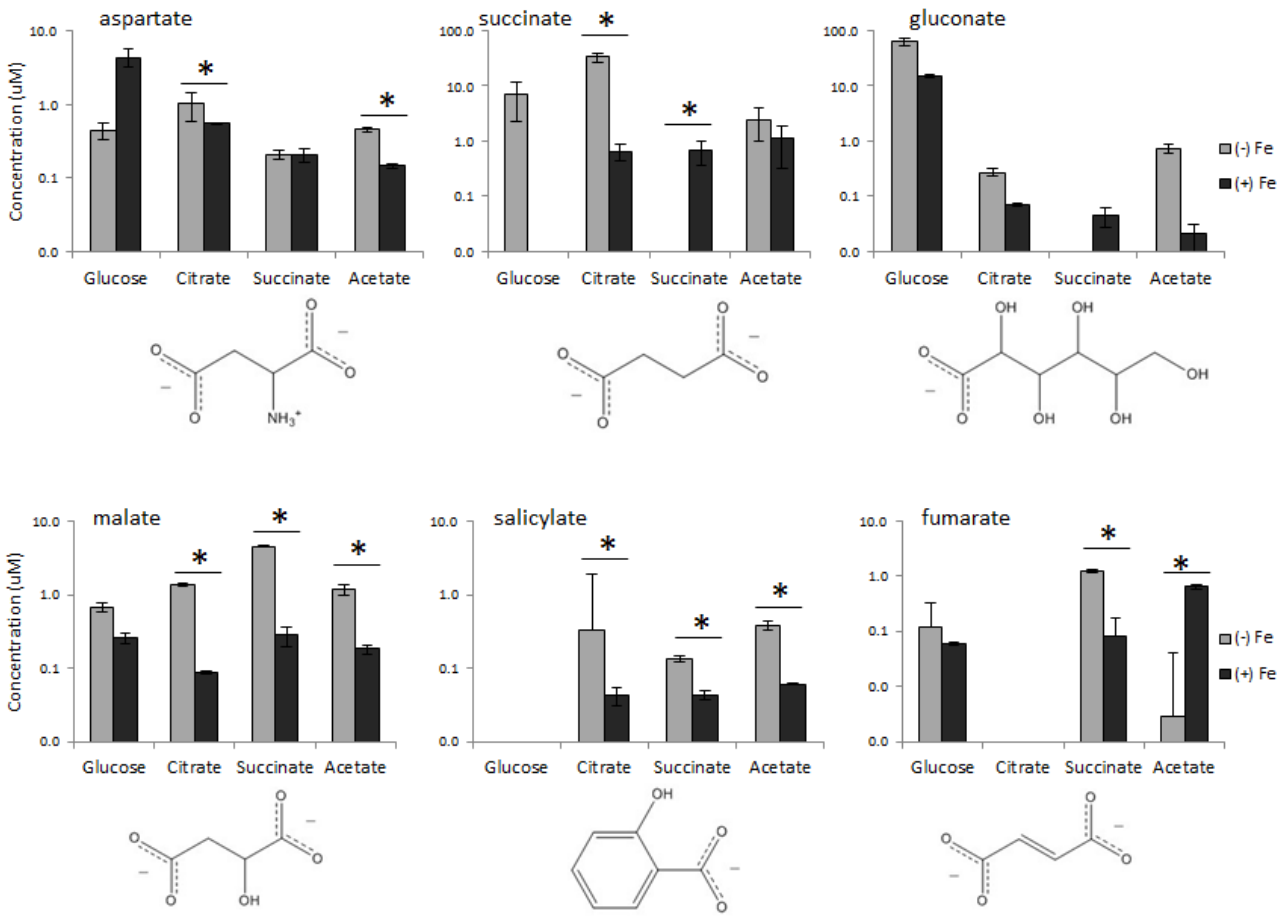

Figure 6. Concentration (µmol L^{-1}) of excreted organic acids (with lowest abundance) in the stationary phase of growth on each substrate (glucose, citrate, succinate and acetate) under Fe-replete (black bars) and Fe-limited (grey bars) conditions. Data shown are mean values ± standard error (n=2). Glucose (+)Fe data was performed by Hua Wei (post doc, Aristilde lab) and are used as a comparison to other carbon substrates and glucose (-)Fe data. Asterisks (*) indicate a statistically significant (p value < 0.05) difference between the two Fe conditions.

Table 2. Extracellular metabolites (μM) at early stationary growth phase reported with standard error (n=2).

Metabolite	Citrate (+)Fe	Citrate (-)Fe	Succinate (+)Fe	Succinate (-)Fe	Acetate (+ Fe)	Acetate (-)Fe	Glucose (+)Fe	Glucose (-)Fe
citrate	--	--	0.390± 0.004	263±6	0.26± 0.03	321±30	12±3	260±30
succinate	0.7±0.2	33±7	--	--	1.1±0.8	2±1	0.0±0.0	7±5
gluconate	0.071± 0.004	0.27±0.04	0.04± 0.02	0.0±0.0	0.02± 0.01	0.7±0.1	14.8±0.8	60±10
2-ketoglutarate	0.22± 0.08	100.7±0.1	0.05± 0.04	2.33±0.09	0.041± 0.005	7.5±0.8	1.4±0.5	0.02±0.01
aspartate	0.54± 0.01	1.0±0.4	0.20± 0.04	0.21±0.03	0.146± 0.009	0.45±0.03	4±1	0.4±0.1
glutamate	0.95± 0.01	8.42±0.02	0.50± 0.03	0.21±0.01	0.148± 0.009	0.9±0.1	110±30	1.2±0.3
hydroxy-benzoate	0.04± 0.01	0.3±2	0.043± 0.006	0.13±0.01	0.060± 0.001	0.38±0.06	0.0±0.0	0.0±0.0
fumarate	0.0±0.0	0.0±0.0	0.08± 0.09	1.21±0.08	0.64± 0.05	0.0±0.0	0.059± 0.003	0.1±0.2
malate	0.086± 0.004	1.36±0.04	0.28± 0.08	4.5±0.1	0.18± 0.03	1.2±0.2	0.25±0.04	0.7±0.1
pyruvate	0.0±0.0	1197.2±0.1	0.03± 0.03	10±1	0.3±0.2	7±1	0.0±0.0	5.0±0.9

In the results presented, overflow metabolism was more pronounced when *P. putida* was grown under Fe-limited conditions, which may be due to a decreased expression of Fe-containing enzymes involved in carbon metabolism and energy conservation as a result of decreased carbon consumption. Fe-containing enzymes involved in carbon metabolism are found in the TCA cycle, most notably aconitase which contains a Fe-S catalytic cluster and converts citrate to aconitate (Shakoury-Elizeh, 2010). Additionally, succinate dehydrogenase, which catalyzes the oxidation of succinate to fumarate, also contains a Fe-S cluster (Shakoury-Elizeh,

2010). Shakoury-Elizeh et al. found a decrease in Fe-containing enzyme activities in the yeast *Saccharomyces cerevisiae*, but surprisingly did not see a consistent disruption of metabolism, especially in amino acid synthesis. That is to say, Fe-S enzymes had lower activity under Fe-limited conditions but still provided enough activity to meet the required demand for amino acid biosynthesis and subsequent metabolism (Shakoury-Elizeh, 2010).

Secreted metabolites appear to correspond with the point of entry of growth substrate in the carbon metabolic network (Figure 4). High levels of gluconate were found in both (+)Fe and (-)Fe media, which are consistent with glucose oxidation to gluconate in the periplasm, or space between the inner and outer membrane, of *P. putida*, before it is transported into the cell (del Castillo, 2007; Schleissner, 1997; Table 2). Additionally, 2-ketoglutarate concentrations were high in citrate, succinate and acetate (-)Fe media (100.7±0.1 μM, 2.33±0.09 μM and 7.5±0.8 μM, respectively), which correspond to the entry points of these metabolites in the TCA cycle (Figure 4). Malate and fumarate in the (-)Fe succinate media were relatively high (4.5±0.1 μM and 1.21±0.08 μM, respectively). This is consistent with the point of entry of succinate in the TCA cycle, the first reactions of which involve forming fumarate and malate (Figure 4). Little pyruvate was found in (+)Fe conditions, but significant amounts were measured in (-)Fe media. Pyruvate secreted in (-)Fe citrate growth media (1197.2±0.1μM) was more than two orders of magnitude higher than in (-)Fe media with glucose, succinate or acetate (5.0±0.9 μM, 10±1 μM and 7±1 μM, respectively; Figure 5). Secreting pyruvate under Fe limitation may be more energetically favorable than routing pyruvate through gluconeogenesis, which requires energy through ATP-consuming reactions (Figure 4).

Mineral dissolution by secreted high- and low-affinity molecules

To elucidate the extent to which the secreted compounds promote mineral dissolution, (-)Fe bacterial secretions were reacted with three different Fe-containing minerals common in soils (Sposito, 1989): hematite, magnetite and goethite. Hematite and magnetite are Fe oxides, while goethite is a Fe oxyhydroxide (Sposito, 1989; Figure 7). A set of control mineral dissolution experiments were first performed with the secreted organic acids mentioned above (10 mM of gluconate, pyruvate, citrate, 2-ketoglutarate, glutamate, succinate, fumarate, malate, aspartate, and citrate), because they have been shown previously to chelate metals from minerals (Duckworth, 2001; Goyne, 2006; Reichard, 2007; Figure 8A), in addition to pyoverdine (100 μM) controls (Figure 8B). Control experiments performed with glucose, succinate and acetate at 100 mM did not dissolve an appreciable amount of Fe from the Fe-bearing minerals (Figure 9). These results suggest that the dissolution of Fe-minerals in glucose-, succinate- or acetate- grown bacterial secretions would be a result of mainly pyoverdine or organic acid secretions, and have little contribution from any substrate remaining in solution.

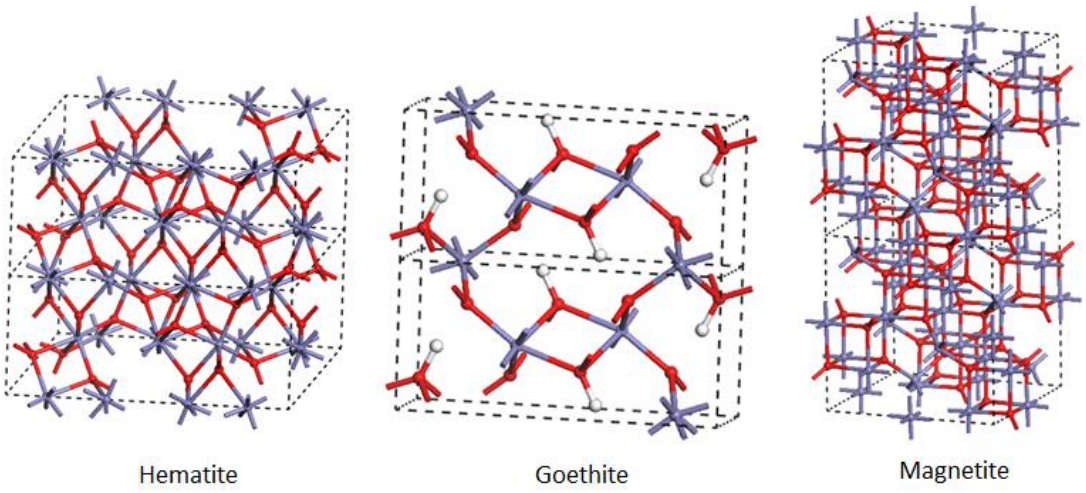

Figure 7. Mineral structure for the three Fe-minerals used in the mineral dissolution experiments (hematite, goethite, and magnetite). Red sticks represent oxygen bonds, purple sticks represent Fe bonds, and white represent hydroxyl groups. Mineral structures obtained from Material Studios.

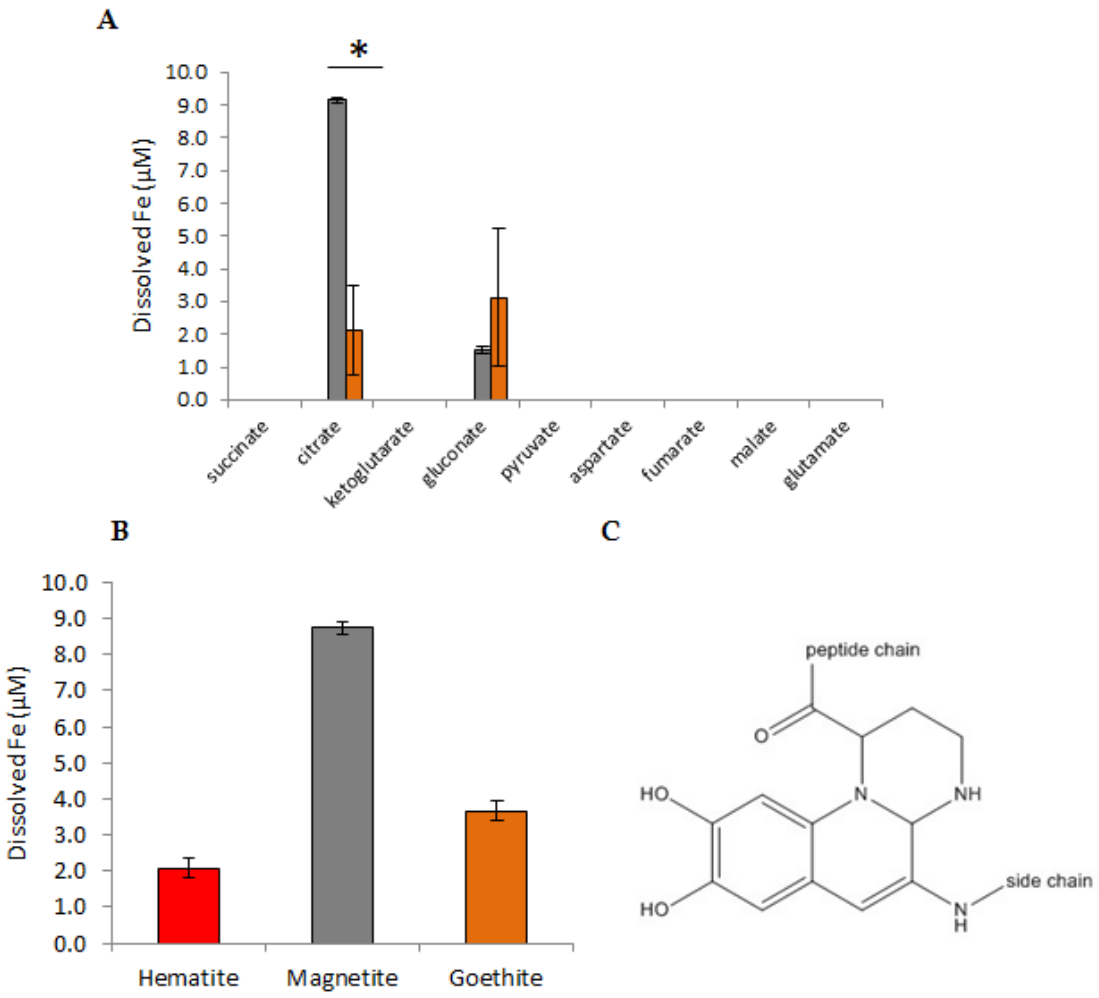

Figure 8. Amount of Fe released (µM) from (A) organic acids found in the extracellular media or from (B) a pyoverdine stock standard (100 µM), with the pyoverdine structure shown (C). Three different Fe-minerals were used: hematite (red), magnetite (grey), goethite (orange). Average values shown with standard error bars (n=2 to 5). An asterisk (*) indicates a statistically significant difference between minerals. For pyoverdine dissolution data, there was a statistically significant difference between Fe dissolved from magnetite and the other two minerals (p value < 0.05), but there was not a significant different between the Fe dissolved between hematite and goethite (p value > 0.05).

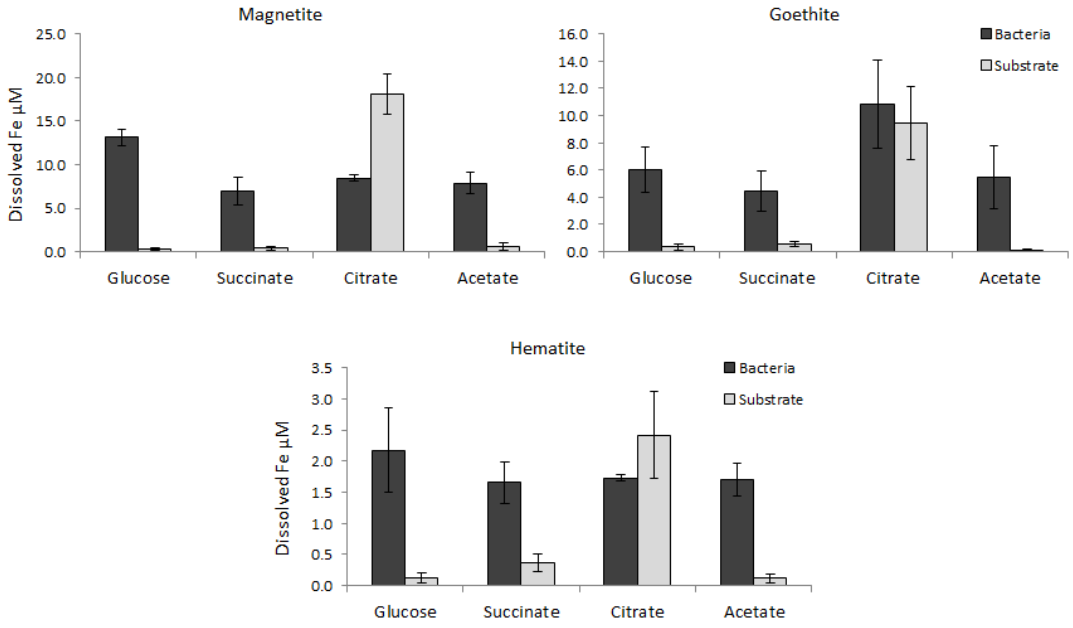

Figure 9. Dissolved Fe (µM) from mineral dissolution experiments with bacterial secretions (dark grey) or 100 mM of substrates (light grey). Substrates used in experiments and for growth to prepare bacterial secretions were glucose, succinate, citrate and acetate. The average is reported with standard error bars (n=2 to 5). An asterisk (*) indicates a statistically significant difference between Fe dissolved in substrate and bacteria secretions (p value <0.05).

Gluconate (10 mM) was able to extract Fe from magnetite and goethite, while all other 10 mM substrates (pyruvate, 2-ketoglutarate, glutamate, succinate, fumarate, malate and aspartate), with the exception of citrate, dissolved negligible to no Fe from each Fe mineral (Figure 8A). Citrate alone was able to dissolve Fe from goethite and magnetite at 10 mM (2.1±1.4 µM and 9.1±0.1 µM, respectively; Figure 8A) and dissolve Fe from hematite, goethite and magnetite at 100 mM concentrations (2.4±0.7 µM, 9.4±2.7 µM and 18.1±2.3 µM, respectively; Figure 9), with magnetite releasing the highest amount of Fe, followed by goethite and hematite (Figure 8A and Figure 9). Citrate has been shown to dissolve Fe from goethite (Reichard, 2007; Cheah, 2003) and other metals, like Cu from chalcopyrite (Goyne, 2006). Also,

citrate at 500 μM,was able to dissolve goethite (2.5 g/L) in the presence of siderophore, desferrioxamine-B (DFO-B; 40 μM). However, goethite dissolution in the presence of only DFO-B was higher than when present with citrate, which may be explained by adsorption competition between organic ligands and siderophore (Reichard, 2007). Citrate is a strong chelator, containing three carboxylate groups which may facilitate dissolution (Ryan, 2001), as may the hydroxyl groups in gluconate. The binding stability of metal complexation by carboxylic acids is increased by the presence of multiple carboxylate groups and their structural arrangement relative to each other and hydroxyl groups in the molecule (Ryan, 2001). Fe(III) complexed with tricarboxylated citrate, dicarboxylated fumarate and monocarboxylated acetate exhibited decreasing binding stability constants (10^{10}, $10^{7.1}$, and $10^{3.4}$, respectively), significantly less stable than the stability constant for Fe-pyoverdine complexes (10^{32}; Albrecht-Gary, 1994). Fe-pyoverdine complexes are more stable than organic ligands complexed with Fe because of the three oxygen containing bidentate groups present in pyoverdine that bind Fe^{3+} (Xiao, 1998).

Bacterial secretions during growth on each substrate were able to dissolve all three Fe minerals. Out of the three minerals, hematite released the least amount of Fe in glucose-, succinate-, citrate- and acetate-grown bacterial secretions (0.12±0.08 μM, 0.37±0.15 μM, 2.42±0.71 μM and 0.12±0.07 μM, respectively; Figure 9). The pyoverdine standard (100 μM) released a comparable amount of Fe from hematite (2.09±0.29 μM; Figure 8B), indicating that the dissolution of hematite in bacterial secretions is mostly, if not entirely, due to pyoverdine. Secretions from glucose-, succinate-, and acetate-grown *P. putida* dissolved the highest amount of Fe from magnetite (0.26±0.13 μM, 0.39±0.27 μM and 0.60±0.39 μM, respectively; Figure 9). Furthermore, secretions from succinate-, citrate-, and acetate-grown *P. putida* dissolved similar amounts of Fe (6.95±1.63 μM, 8.46±0.41 μM, and 7.87±1.23 μM, respectively; Figure 9) to Fe

released by the pyoverdine standard (8.73±0.16 μM; Figure 8B). The glucose-grown bacterial secretion dissolved more Fe from magnetite (13.10±0.93 μM; Figure 9) than the pyoverdine standard (8.73±0.16 μM; Figure 8B), indicating the levels of secreted organic acids in (-)Fe glucose media (mainly gluconate and citrate) may act in concert with pyoverdine to augment magnetite dissolution. In terms of goethite dissolution, glucose-, succinate- and acetate-grown bacterial secretions led to higher dissolved Fe (0.35±0.22 μM, 0.57±0.19 μM and 0.10±0.07 μM, respectively; Figure 9) than pyoverdine alone (3.66±0.26 μM; Figure 8B). This indicates the participation of extracellular media components in the dissolution of goethite in addition to pyoverdine. More Fe was released from goethite in the citrate-grown bacterial secretion (9.42±2.68 μM; Figure 9) than in the presence of the other three bacterial secretions. The dissimilarities in dissolution between minerals may be a result of structural differences. Magnetite contains both Fe(II) and Fe(III) (Sposito, 1989) resulting in more open spaces, which may facilitate greater accessibility of ligand binding to Fe metal centers, and thus, making Fe more readily released (Figure 7). Hematite and goethite both contain Fe(III) (Sposito, 1989), but goethite is an Fe oxyhydroxide with hydroxyl groups, which may support hydrogen bonding to organic acids. Accordingly, more goethite dissolution was measured than hematite dissolution (Figure 8 and Figure 9).

The results presented in this section demonstrated that the production of pyoverdine and organic acids is dependent both on growth substrate and Fe conditions. The extracellular metabolite pools for citrate, succinate, glucose and acetate are likely a response to reduced activity of Fe-containing enzymes and a coping strategy to conserve energy until Fe availability is favorable for carbon uptake, metabolism and biomass production. Citrate was able to dissolve more Fe from each Fe-mineral, which is consistent with its tricarboxylic acid structure,

facilitating a high affinity for metal ions. The organic secretions outlined here contribute to metal-acquisition strategies of *P. putida,* the composition of which are closely associated with the point of entry of the growth substrate in the central carbon metabolism. These results advance our understanding of the differing metabolic responses of *P. putida* in environmental habitats of differing carbon sources and Fe availability.

CHAPTER 4

IRON-DEPENDENT METABOLISM OF GLUCOSE

Intracellular quantification of metabolites

The difference in the bacterial secretions in (+)Fe and (-)Fe growth conditions presented in the previous section indicated a rerouting of consumed organic substrates to promote the secretion of high affinity pyoverdine in addition to small organic acids under Fe limitation. Fe-limited glucose-grown *P. putida* secreted less pyoverdine and organic acids, indicating a greater substrate to biomass conversion when glucose was the sole carbon source.

As a first look at the metabolite consequences of Fe conditions, intracellular metabolites were quantified to determine the relative pools of metabolites under (-) and (+)Fe conditions. Concentrations of 6-phosphogluconate, citrate and glutamate were elevated under Fe-limited conditions (0.54±0.03 μM, 1.89±0.16 μM and 5.48±0.79 μM, respectively; Figure 10). The initial metabolism of citrate is catalyzed by Fe-S cluster containing enzymes (aconitase), which may account for the accumulation of this metabolite (Shakoury-Elizeh, 2010). Glutamate accumulation may be as a result of pooling for siderophore formation, as both glutamate and glutamine, an amino acid formed from glutamate, have been shown in the structure of pyoverdines from *P. putida* (Meyer, 2008). 6-Phosphogluconate also had an increased intracellular concentration under Fe-limited conditions, indicating a possible direct or indirect Fe regulation of the reactions that metabolize 6-phosphogluconate further. The accumulation of both 6-phosphogluconate and citrate when *P. putida* had limited Fe indicates a possible bottleneck in the central carbon metabolism at the ED and PP pathways and at the beginning of the TCA cycle, which may be a result of altered carbon fluxes through the central carbon metabolism.

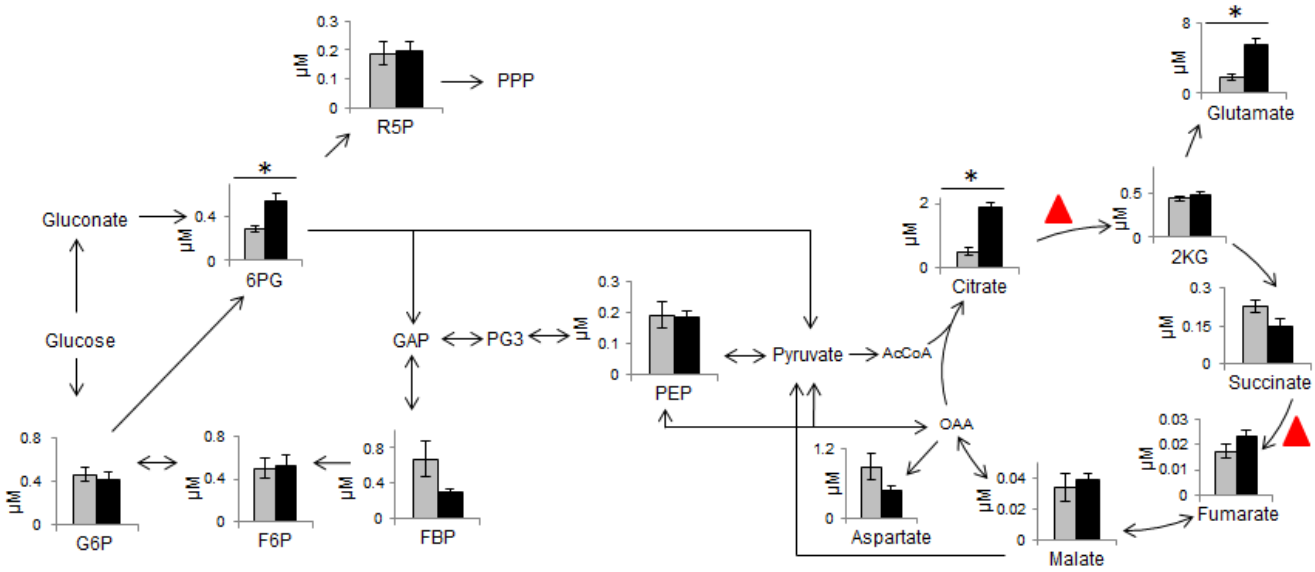

Figure 10. Intracellular concentrations (µM) of target central carbon metabolites under (+)Fe (grey) and (-)Fe (black) conditions. Data shown are averages with standard error (n=3). Red triangles mark reactions with enzymes containing Fe-S clusters. An asterisk (*) indicates a statistically significant difference between the intracellular concentrations in (+)Fe and (-)Fe conditions (p value < 0.05). Abbreviations are as follows: glucose-6-phosphate, G6P; fructose-6-phosphate, F6P; fructose-1,6-bisphosphate, FBP; 6-phosphogluconate, 6PG; glyceraldehyde-3-phosphate, GAP; 3-phosphoglycerate, 3PG; phosphoenolpyruvate, PEP; 2-ketoglutarate, 2KG; pentose phosphate pathway, PPP.

Kinetic and steady-state isotopic labeling experiments

To understand the significance of these elevated metabolites in the central carbon metabolism, kinetic isotopic tracer experiments with fully labeled [U-^{13}C] glucose were performed to elucidate further the changes in the intracellular incorporation of glucose under (+)Fe and (-)Fe growth conditions. This technique has been used previously to decipher the metabolic pathways in bacteria whereby unique labeling profiles can reveal pathways involved in glucose metabolism (Amador-Noguez, 2010; Crown, 2012; Antoniewicz, 2013). Under both Fe conditions, the ED pathway was favored for glucose metabolism (Figure 11). Due to the absence of the EMP pathway, *P. putida* utilizes the ED pathway to metabolize glucose to pyruvate and glyceraldehyde-3-phosphate. The ED pathway was first noted in Pseudomonads decades ago,

and has been verified through genomics and metabolomics (Blank, 2008; Puchalka, 2008; del Castillo, 2007). There are three ways that *P. putida* can metabolize glucose to 6-phosphogluconate, the key metabolite in the ED pathway: glucose kinase phosphorylates glucose to glucose-6 phosphate, which can then be converted to 6-phosphogluconate; following oxidation of glucose to gluconate, gluconokinase phosphorylates gluconate to 6-phosphogluconate; gluconate can be oxidized further to 2-ketogluconate, which goes on to form 6-phosphogluconate (del Castillo, 2007; Figure 4). The subsequent step in the ED pathway entails the conversion of 6-phosphogluconate to 2-keto-3-deoxy-6-phosphogluconate, which breaks into pyruvate and glyceraldehyde-3 phosphate, an important branching metabolite that feeds into the PP pathway (del Castillo, 2007; Figure 4). Similar rates of incorporation of [U-^{13}C] glucose (Figure 11) were measured for 6-phosphogluconate, gluconate, glucose-6-phosphate, dihydroxyacetone-phosphate, 3-phosphoglycerate, and pyruvate. Whereas the rate of complete labeling of phosphoenolpyruvate, fructose-1,6-bisphosphate, and fructose-6-phosphate was slower, indicating a smaller flux towards these metabolites (Figure 11). A smaller flux to phosphoenolpyruvate, fructose-1,6-bisphosphate, and fructose-6-phosphate has been noted previously in flux analyses of *P. putida* grown on glucose with sufficient Fe (Blank, 2008; del Castillo, 2007; Puchalka, 2008).

Kinetics for TCA cycle intermediates were also measured for both Fe conditions (Figure 12). All measured metabolites (acetyl-CoA, aspartate, citrate, glutamate, 2-ketoglutarate, fumarate, and succinate) became fully labeled over the sixty minute measuring period. At the end of an hour, metabolites in the (+)Fe condition contained less 0-labeled glucose than in the (-)Fe condition. Succinate, fumarate and 2-ketoglutarate contained 20%, on average, of 0-labeled compound after one hour under Fe limited conditions (Figure 12) compared to the nearly 5%, on

average, of 0-labeled compound when grown with sufficient Fe (Figure 12). This labeling pattern agrees with the metabolic bottleneck intracellular citrate observed when *P. putida* was grown under Fe limitation (Figure 10). Since citrate labeling is similar under both Fe conditions, metabolism to citrate does not appear to be disrupted when Fe is limited, but the reactions following the formation of citrate appear to be reduced. This may be due to the Fe-dependent enzymes, mentioned earlier, responsible for metabolizing citrate to 2-ketoglutarate and succinate to fumarate (Shakoury-Elizeh, 2010). Labeling incorporation into PP pathway metabolites was also monitored under both Fe conditions (Figure 13). No significant difference was noted between xylulose-5-phosphate, ribose-5-phosphate or sedoheptulose-7-phosphate in the Fe conditions.

Kinetic labeling experiments using [1,2-^{13}C] labeled glucose were also performed to elucidate any changes in labeling patterns that were indistinguishable with fully labeled glucose. Again, labeling patterns support the ED pathway as the primary route of carbon metabolism (Figure 14) under (+)Fe and (-)Fe growth conditions. Gluconate (90%) incorporates the 2-labeled glucose at a higher rate than G6P (65%), while F6P contains a high amount of 0-labeled carbons (more than 70%) at the end of one hour (Figure 14). Figure 15 shows a schematic for the possible labeling patterns of glycolytic and ED pathway metabolites when *P. putida* is grown on [1,2-^{13}C] glucose. 6-PG splits into GAP and pyruvate which accounts for the high amount of 0-labeled GAP (in equilibrium with DHAP) and the elevated levels of 2-labeled pyruvate (Figure 15). Consistent with the downstream catabolism of 0-labeled GAP through the remaining steps of glycolysis to form pyruvate, 0-labeled pyruvate was also measured.

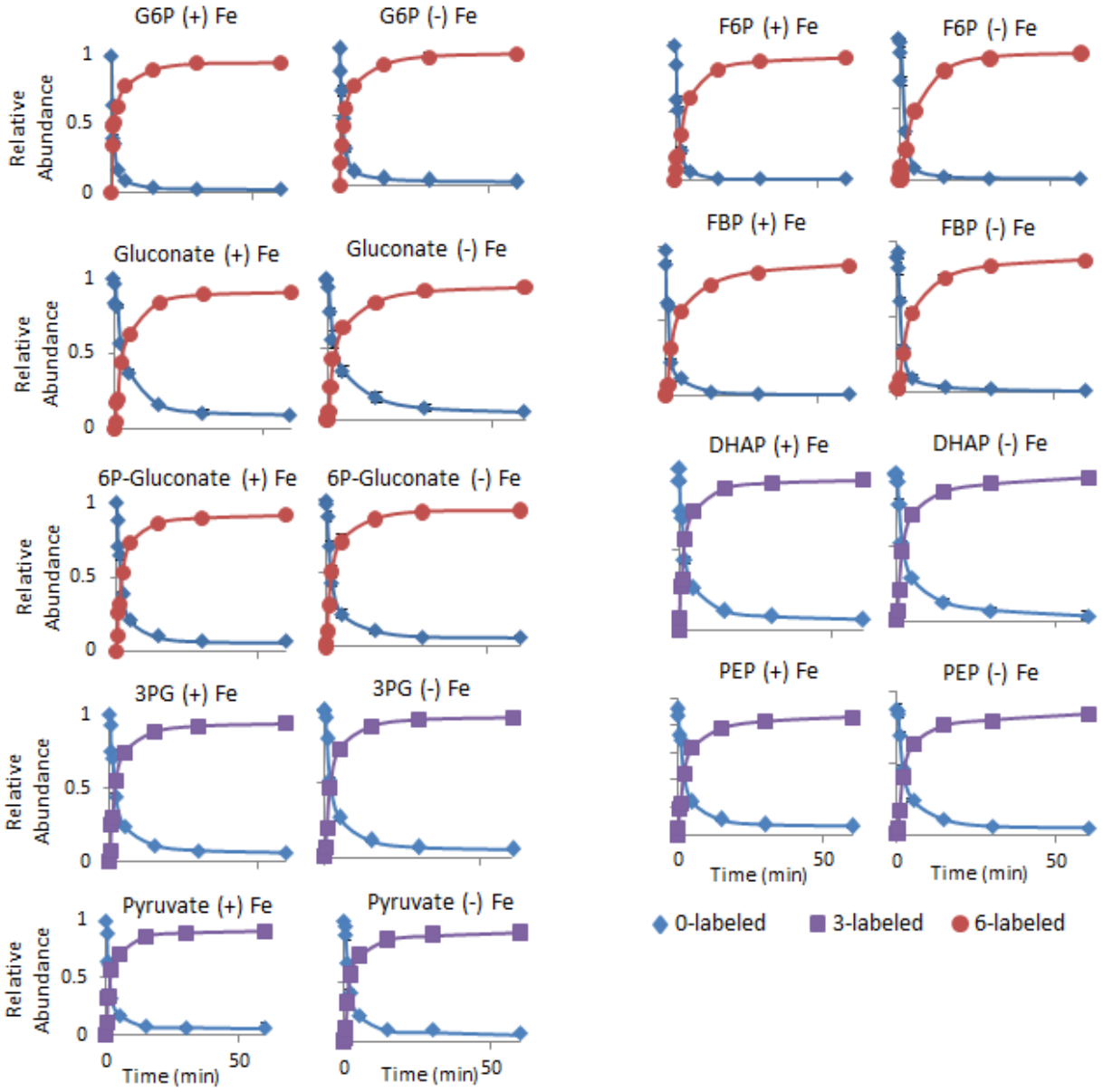

Figure 11. Fully labeled glucose kinetics data for glycolytic and Entner-Doudoroff pathway metabolites under (+)Fe and (-)Fe growth conditions over the span of one hour with standard deviation error bars (n=3). Only kinetics of 0- and fully-labeled carbons are shown. Abbreviations are as follows: glucose-6-phosphate, G6P; 6-phosphogluconate, 6P-gluconate; fructose-6-phosphate, F6P; fructose-1,6-bisphosphate, FBP; dihydroxyacetone phosphate, DHAP; 3-phosphoglycerate, 3PG; phosphoenolpyruvate, PEP.

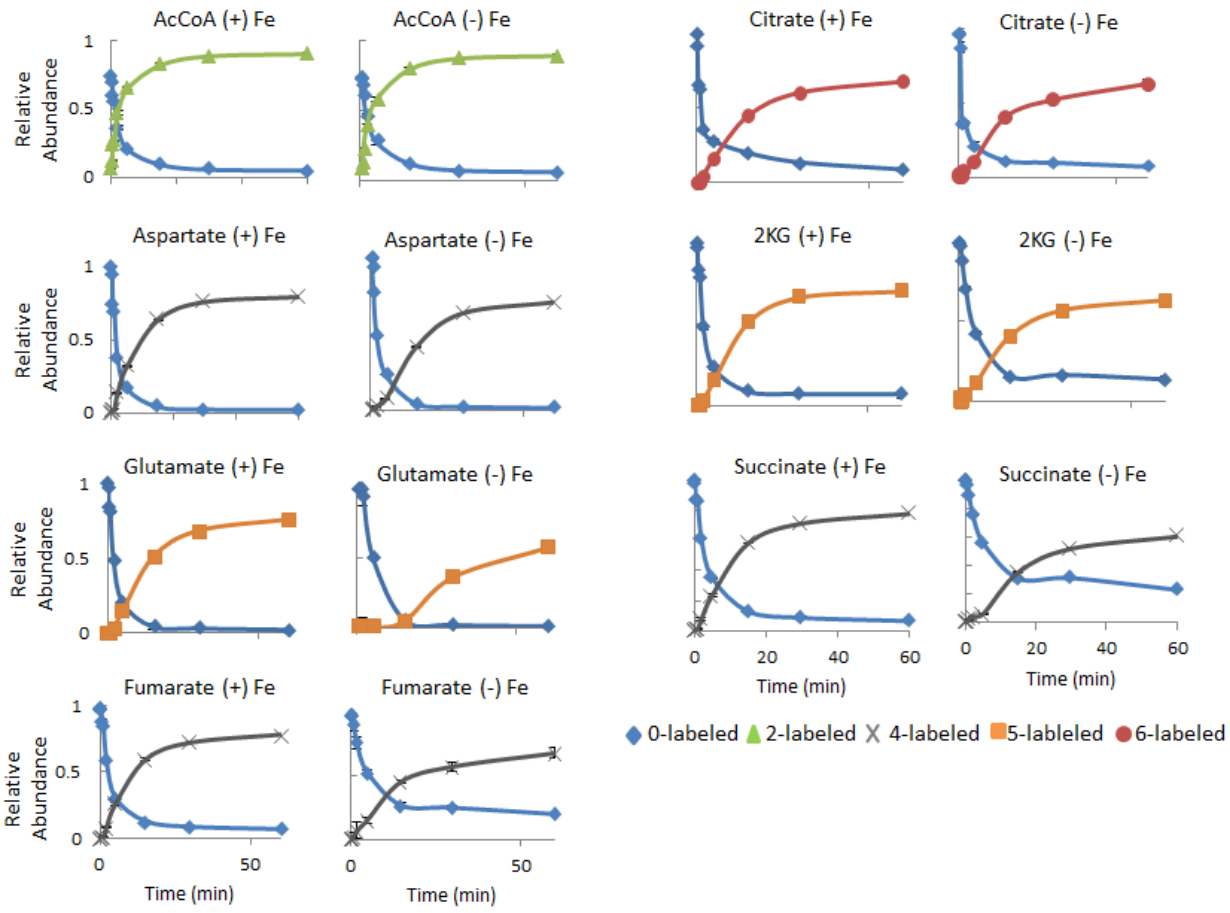

Figure 12. Fully labeled glucose kinetics data for TCA cycle metabolites, in addition to the amino acids aspartate and glutamate, under (+)Fe and (-)Fe growth conditions over the span of one hour with standard deviation error bars (n=3). Only kinetics of 0- and fully-labeled carbons are shown. Abbreviations are as follows: acetyl coenzyme A, AcCoA; 2-ketoglutarate, 2KG.

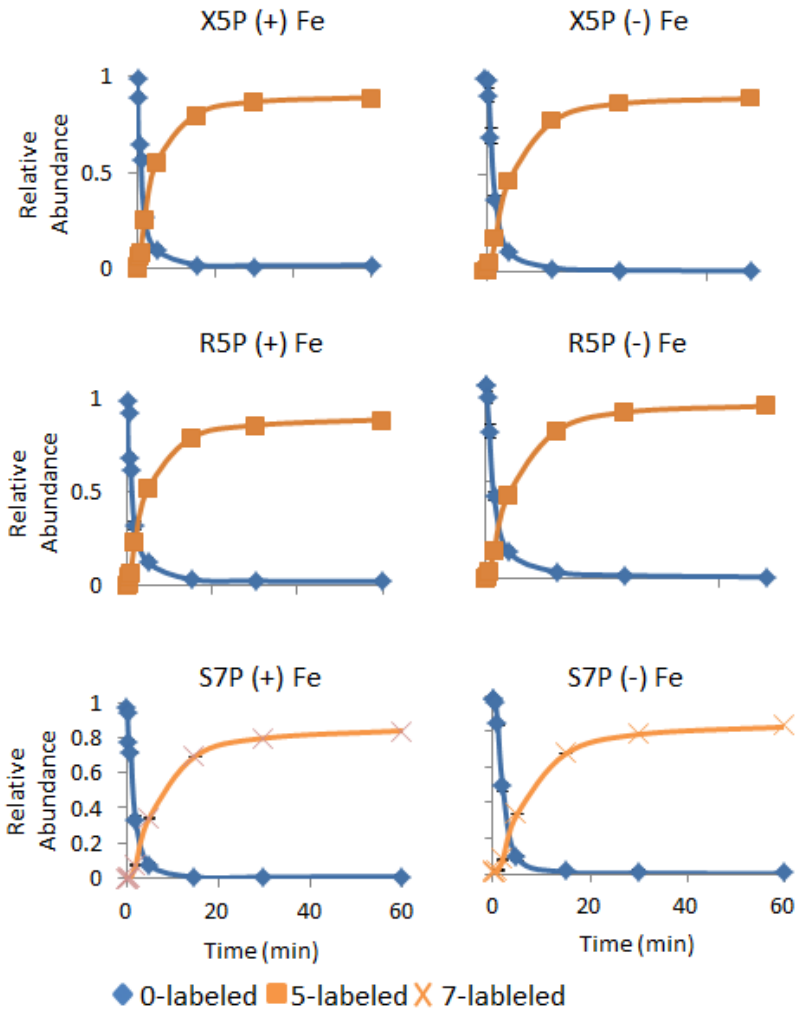

Figure 13. Fully labeled glucose kinetics data for pentose phosphate pathway metabolites under (+)Fe and (-)Fe growth conditions over the span of one hour with standard deviation error bars (n=3). Only kinetics of 0- and fully-labeled carbons are shown. Abbreviations are as follows: xylulose-5-phosphate, X5P; ribose-5-phosphate, R5P; sedoheptulose-7-phosphate, S7P.

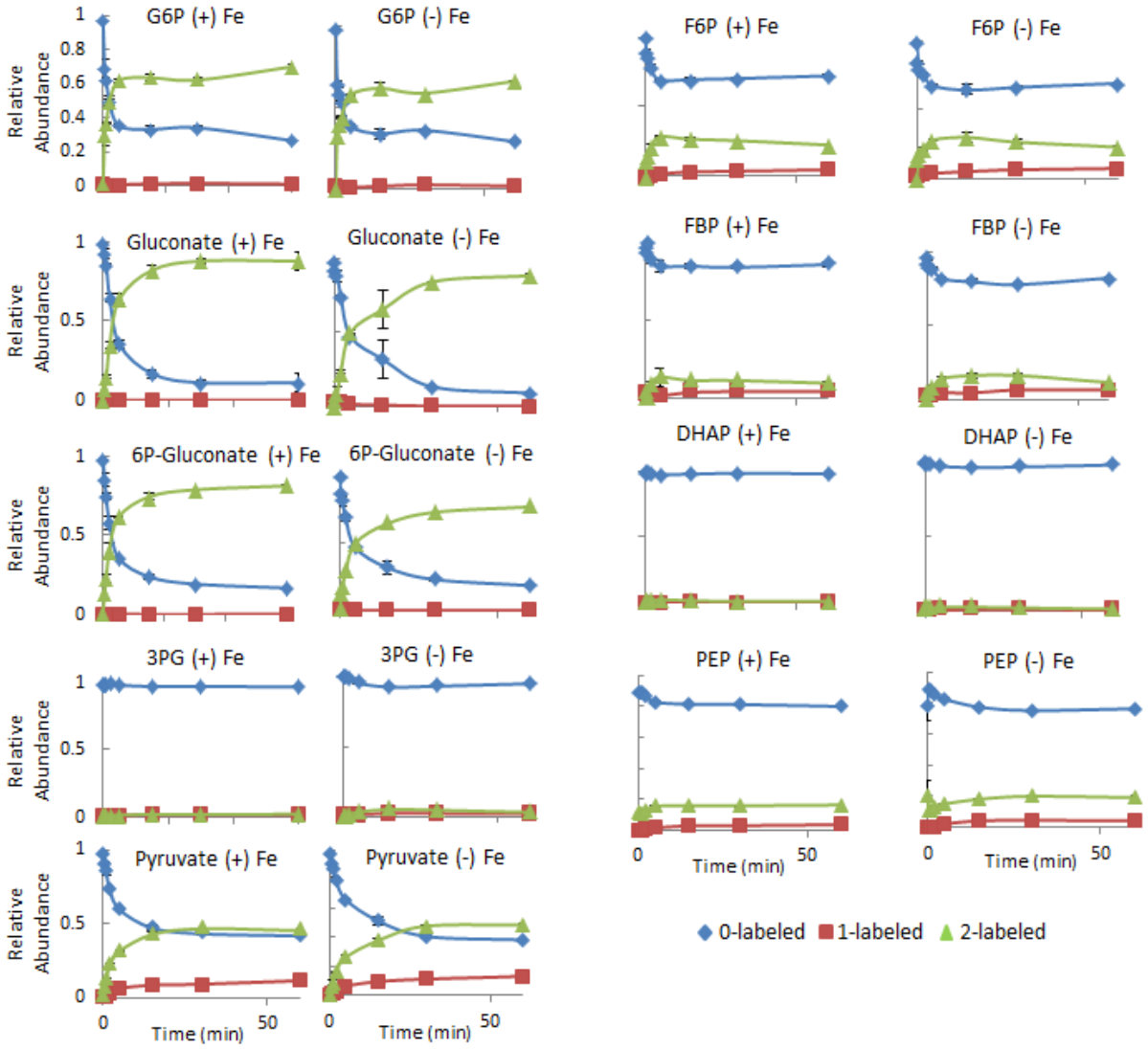

Figure 14. [1,2-^{13}C] glucose kinetics data for glycolytic and Entner-Doudoroff pathway metabolites under (+)Fe and (-)Fe growth condition. Only kinetics of 0-, 1- and 2- labeled carbons are shown. Averages shown with standard deviation bars (n=2). Abbreviations are as follows: glucose-6-phosphate, G6P; 6-phosphogluconate, 6P-gluconate; fructose-6-phosphate, F6P; fructose-1,6-bisphosphate, FBP; dihydroxyacetone phosphate, DHAP; 3-phosphoglycerate, 3PG; phosphoenolpyruvate, PEP.

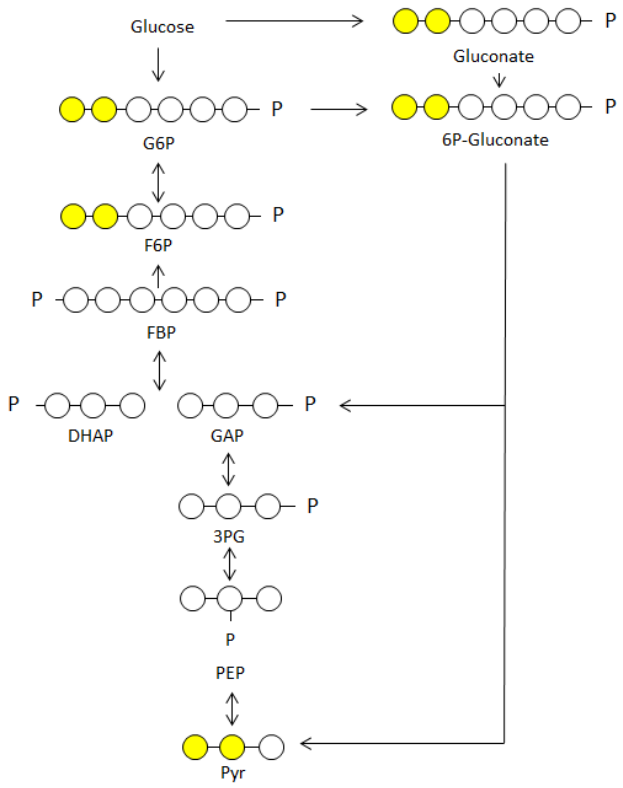

Figure 15. Labeling schematic for glycolytic and Entner-Doudoroff pathway metabolites from one cycle of [1,2-^{13}C] glucose through each pathway. The solid yellow circles indicate a labeled carbon while the white circles represent unlabeled carbons. Abbreviations are as follows: glucose-6-phosphate, G6P; fructose-6-phosphate, F6P; fructose-1,6-bisphosphate, FBP; dihydroxyacetone phosphate, DHAP; glyceraldehyde-3-phosphate, GAP; 3-phosphoglycerate, 3PG; phosphoenolpyruvate, PEP; pyruvate, Pyr; 6-phosphogluconate, 6P-gluconate.

Steady-state experiments were carried out with [1,2-^{13}C] glucose for use in MFA. *P. putida* was harvested during early exponential phase (OD_{600} 0.6-0.8). At this point, the system was taken to be in pseudo steady-state; that is the change in metabolite concentration and fluxes remained constant. Phosphoenolpyruvate (PEP) and pyruvate showed slightly different labeling signatures in the two Fe conditions (Figure 16). With limited Fe, PEP contained 75% 0-labeled carbons compared to about 80% in sufficient Fe. Additionally, there was more 2-labeled PEP (20%) under Fe-limited conditions than Fe-replete conditions (15%). The slight difference in PEP labeling at steady-state suggests different fluxes to PEP in (-)Fe conditions compared to

(+)Fe conditions. Most of the metabolites (G6P, gluconate, 6-PG, F6P, 3PG, FBP, DHAP and pyruvate) did not show a significant change in steady-state labeling profiles across the two Fe conditions (Figure 16). There was a significant change in the labeling profile of PEP in (-)Fe conditions compared to (+)Fe conditions. With limited Fe, PEP had more 2-labeling and less 0-labeling. This indicates a different route of carbon flux to PEP under Fe-limited conditions, which is interesting given that PEP is a precursor to aromatic amino acids. The aromatic amino acid tyrosine is a known precursor to the chromophoric section of pyoverdine (Stintzi, 1996). PEP can be synthesized from 3-phosphoglycerate (3PG) or oxaloacetate (OAA) (Figure 17). It appears under (+)Fe, PEP is mainly formed from 3PG. 3PG and PEP are both 3-carbon compounds, so no loss of carbon would result in a high amount of 0-labeled PEP forming from 3PG (Figure 17). Under (-)Fe, it is likely that the flux from OAA to PEP is higher than in (+)Fe conditions. Depending on where the carbons are labeled in OAA, a 3-labeled OAA could result in a 2-labeled PEP, as OAA loses a carbon to form PEP (Figure 17). Previous research looking at the flux of glucose in *P. putida* showed a high flux of PEP forming from 3-PG, with little contribution from OAA (del Castillo, 2007; Puchalka, 2008; Blank, 2008).

[1,2-^{13}C] labeled glucose kinetics data for TCA cycle intermediates reveal an active TCA cycle flowing in the oxidative direction, from citrate to OAA. Aspartate (used as a stand in for OAA labeling because aspartate and OAA were assumed to be in equilibrium), citrate, 2-ketoglutarate and glutamate have consistent labeling patterns with what is predicted with [1,2-^{13}C] glucose incorporation (Figure 18). Succinate has a higher amount of 0-labeled carbon in both (+)Fe and (-)Fe conditions (40% on average), as does fumarate, but to a greater extent (60% on average). This indicates a decreased flux around the TCA cycle, with OAA primarily being formed from PEP or pyruvate, more so than fumarate. The presence of higher levels of 1-labeled

fumarate may indicate an active glyoxylate shunt under both conditions, the labeling pattern from the glyoxylate shunt would primarily produce 1-labeled malate (Figure 19), which could then form fumarate. Under sufficient Fe conditions, the glyoxylate shunt is typically inactive (del Castillo, 2007; Puchalka, 2008; Blank, 2008), but may become active under Fe-limited conditions or different environmental stresses. The higher amount of 0-labeled fumarate and succinate were also present in (+) and (-)Fe steady-state measurements (Figure 20). Citrate contained an average of 10% 3-labeled carbons and an average of 5% 4-labeled carbons, which would form from 3-labeled OAA and 1-labeled acetyl-CoA (Figure 20).

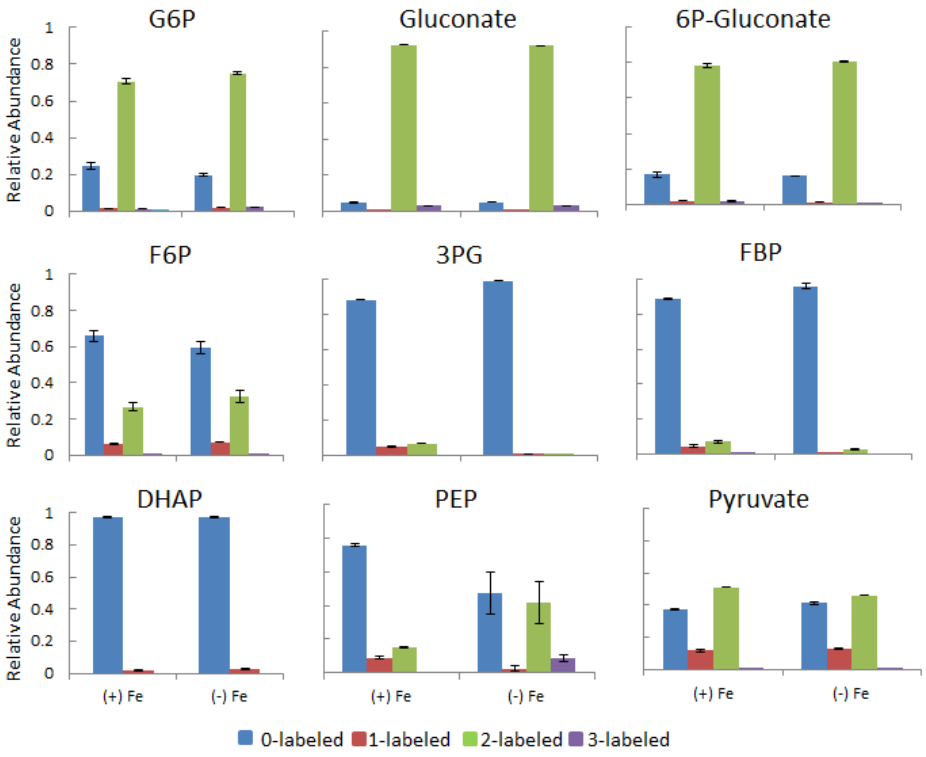

Figure 16. Steady-state labeling data for (+) and (-)Fe conditions with *P. putida* grown on [1,2-^{13}C] glucose to early exponential stage. Values shown are averages between two biological duplicates with standard deviation error bars. Labeled signifies simply amount of carbons labeled, but does not designate which carbons are labeled in each metabolites. Abbreviations are as follows: glucose-6-phosphate, G6P; fructose-6-phosphate, F6P; fructose-1,6-bisphosphate, FBP; dihydroxyacetone phosphate, DHAP; glyceraldehyde-3-phosphate, GAP; 3-phosphoglycerate, 3PG; phosphoenolpyruvate, PEP; 6-phosphogluconate, 6P-gluconate.

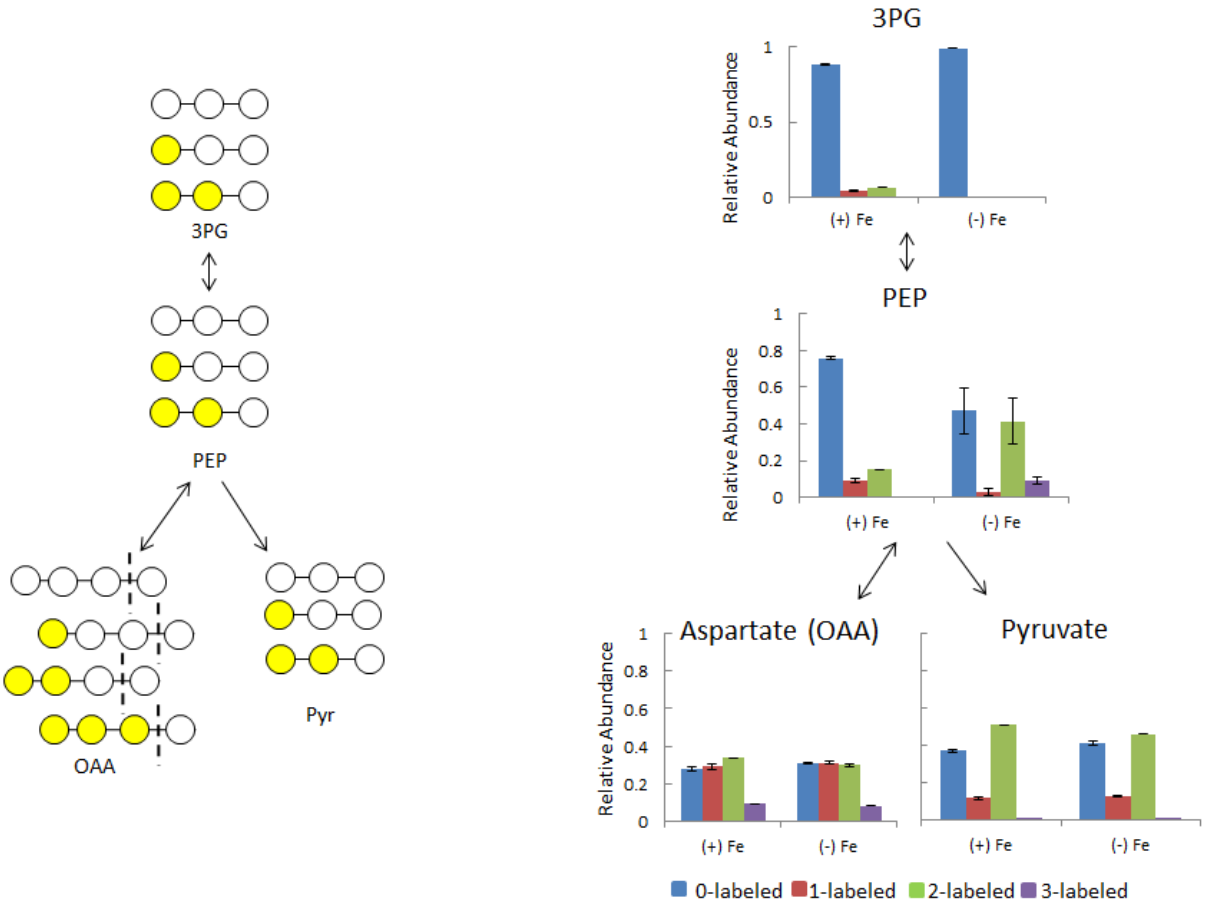

Figure 17. Schematic and labeling patterns for the formation of PEP. Steady state labeling data shown for (+)Fe and (-)Fe growth conditions on [1,2-^{13}C] glucose. Aspartate labeling is shown as a stand in for oxaloacetate labeling, which was not measurable via LC-MS. Abbreviations are as follows: 3-phosphoglycerate, 3PG; phosphoenolpyruvate, PEP; pyruvate, Pyr; oxaloacetate, OAA.

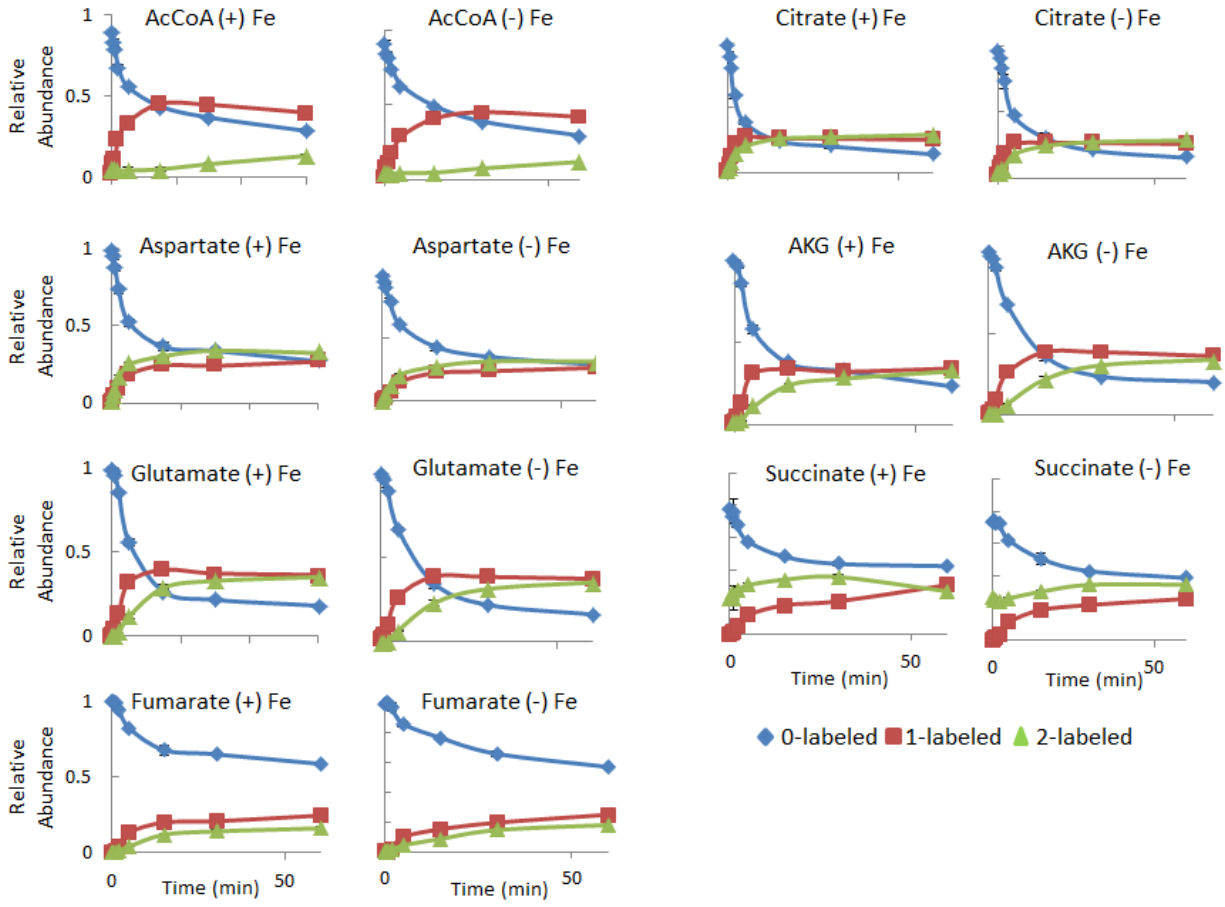

Figure 18. [1,2-^{13}C] glucose kinetics data from (+)Fe and (-)Fe growth conditions of TCA cycle metabolites. Only kinetics of 0-, 1- and 2- labeled carbons are shown. Averages are shown with standard deviations (n=2). Abbreviations are as follows: acetyl coenzyme A, AcCoA; 2-ketoglutarate, AKG.

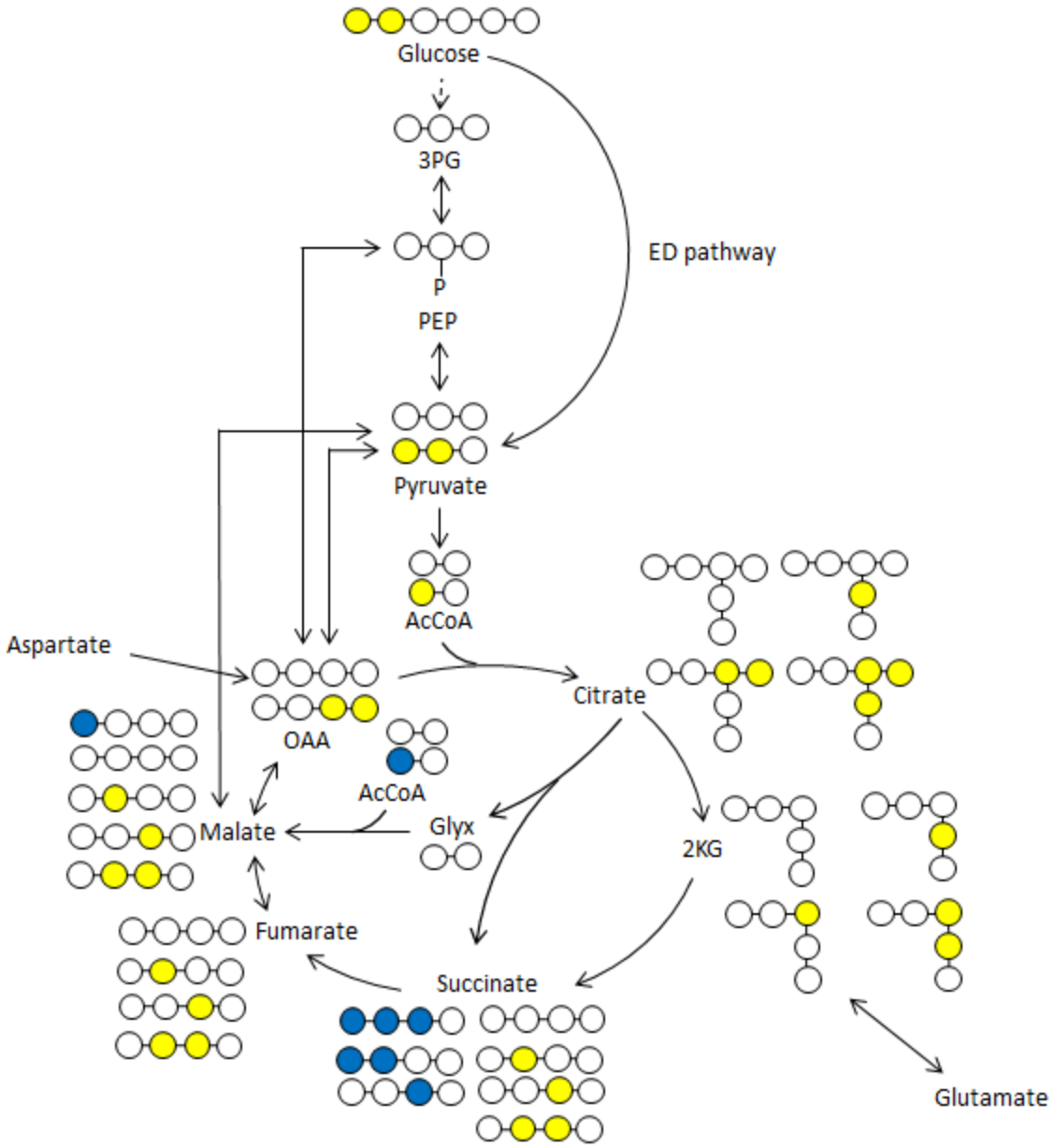

Figure 19. Schematic for labeling possibilities for one cycle of metabolized [1,2-^{13}C] glucose around the TCA cycle. Yellow represents carbon labeled from one cycle of the TCA cycle, while blue represents labeled carbons from the glyoxylate shunt. The dashed line between glucose and 3PG represents a truncated glycolysis, which produces 0-labeld PEP. The ED pathway produces 2-labeled pyruvate. Abbreviations are as follows: 3-phosphoglycerate, 3PG; phosphoenolpyruvate, PEP; pyruvate, Pyr; 2-ketoglutarate, 2KG; glutamate, Glu; aspartate, Asp; oxaloacetate, OAA; glyoxylate, Glyx; acetyl coenzyme A, AcCoA.

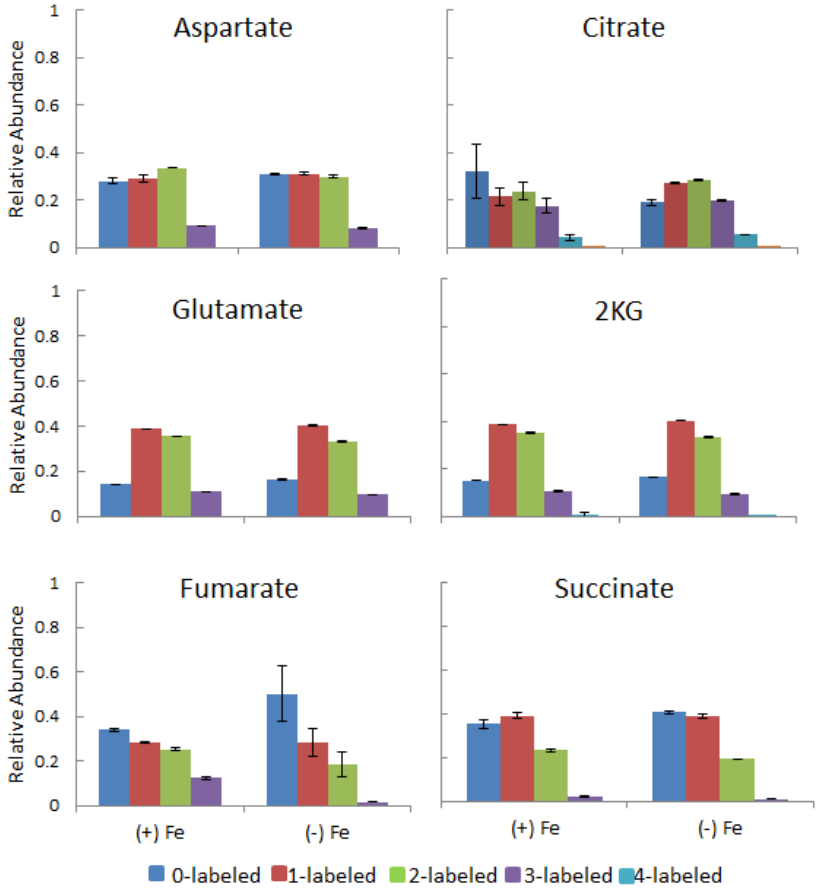

Figure 20. Steady state labeling for TCA cycle compounds during early exponential growth phase for (+)Fe and (-)Fe growth conditions on [1,2-^{13}C] glucose. Samples are averages of two biological replicates with standard deviation error bars. Abbreviations are as follows: 2-ketoglutarate, 2KG.

Pentose phosphate pathway compounds contained similar labeling patterns in both Fe conditions (Figure 21). X5P, R5P, and S7P all contained mostly 0-lableled carbons (average of 80%) after one hour. This indicates a small flux to the PP pathway compared to other pathways in the central carbon metabolism. The PP pathway, responsible for forming nucleotides and generating NADPH, an important anabolic cofactor and regulator of oxidative stress (Chavarria, 2012), has been shown to have a very small flux of carbon in *P. putida* when grown on glucose and other carbon sources (del Castillo, 2007; Puchalka, 2008; Blank, 2008; Fuhrer, 2005). The

amount of 2-labeled carbons quickly increases in X5P and R5P (Figure 21), in both Fe conditions, initially, but was then surpassed by 1-labeled carbons after 30 minutes. This indicates that initially, X5P and R5P were formed from the PP pathway, fed by glycolytic metabolites, and then later, these two compounds formed from 6-phosphogluconate (Figure 22). The schematic in Figure 22 shows the labeling that would occur if X5P and R5P were formed from 6-phosphogluconate, forming from the PP pathway would consist of a 2-labeled F6P (from 2-labeled G6P) combining with a 0-labeled GAP to form 2-labeled X5P. At steady-state (Figure 23), there is more 1-labeled X5P and R5P than 0-labeled, matching the kinetics data. There was a small amount of 3-labeled S7P present at steady-state, which may form from a 2-labeled X5P combining with a 1-labeled R5P or a 2-labeled R5P combining with a 1-labeled X5P (Figure 22).

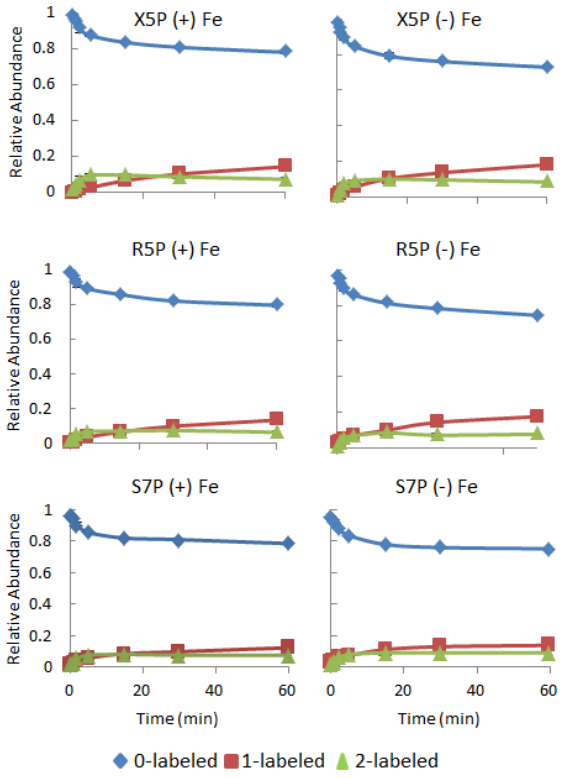

Figure 21. [1,2-^{13}C] glucose kinetics data for (+)Fe and (-)Fe conditions of pentose phosphate pathway metabolites. Only kinetics of 0-, 1- and 2- labeled carbons are shown. Averages are shown with standard deviation error bars (n=2). Abbreviations are as follows: xylulose-5-phosphate, X5P; ribose-5-phosphate, R5P; sedoheptulose-7-phosphate, S7P; sedoheptulose-1,7-bisphosphate, SBP; octulose-8-phosphate, O8P.

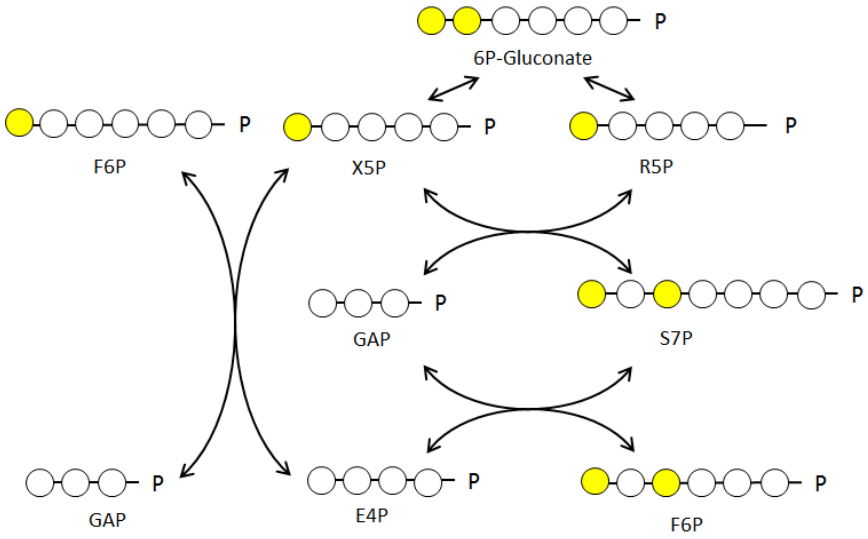

Figure 22. Labeling schematic for the pentose phosphate pathway of metabolized [1,2-^{13}C] glucose. Labeled carbons are highlighted in yellow while unlabeled carbons are white. Abbreviations are as follows: xylulose-5-phosphate, X5P; ribose-5-phosphate, R5P; sedoheptulose-7-phosphate, S7P; sedoheptulose-1,7-bisphosphate, SBP; octulose-8-phosphate, O8P; octulose-1,8-bisphosphate, OBP; dihydroxyacetone phosphate, DHAP; glyceraldehyde-3-phosphate, GAP; fructose-6-phosphate, F6P, 6-phosphogluconate, 6P-gluconate.

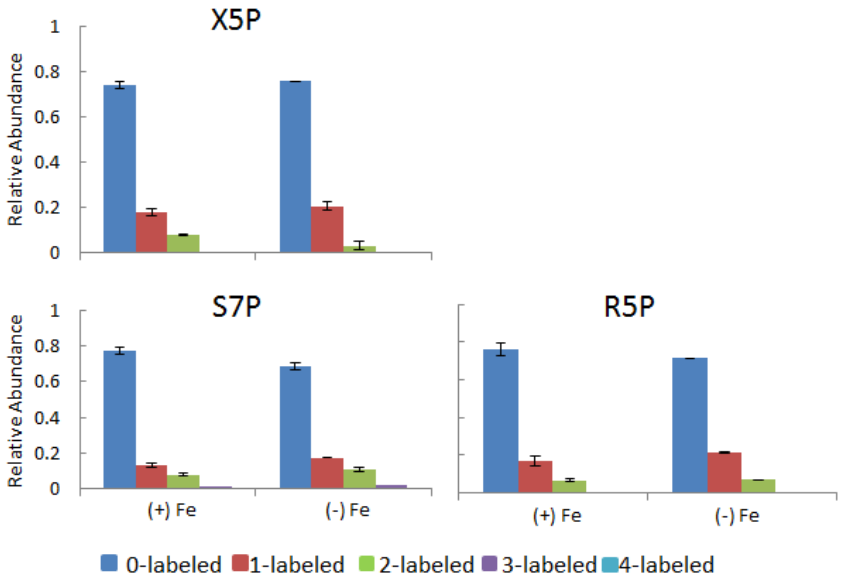

Figure 23. [1,2-^{13}C] glucose steady state data for (+)Fe conditions of pentose phosphate pathway metabolites. Averages are shown with standard deviation error bars (n=2). Abbreviations are as follows: xylulose-5-phosphate, X5P; ribose-5-phosphate, R5P; sedoheptulose-7-phosphate, S7P; sedoheptulose-1,7-bisphosphate, SBP; octulose-8-phosphate, O8P.

Identification of untargeted metabolites

The untargeted method used to analyze the kinetic and steady-state data is capable of detecting unknown compounds in addition to known metabolites, a useful tool when performing intracellular metabolomics (Mapelli, 2008; Clasquin, 2011). While the central carbon metabolism of *P. putida* KT2440 has been well studied, there remains the possibility for discovering new metabolic pathways or metabolites (Winsor, 2011). Two compounds (sedheptulose-1,7-bisphosphate and octulose-8-phosphate) shown to be present in eukaryotic cells (Clasquin, 2011) were found intracellularly in *P. putida* in both kinetics and steady-state experiments (Figure 24A, 24B and 25). These compounds are involved in riboneogenesis, a thermodynamically favored synthesis of ribose that does not require NADPH formation (Clasquin, 2011).

There are two potential pathways for the formation of octulose-8-phosphate (O8P) and sedoheptulose-1,7-bisphosphate (SBP). O8P may be formed from fructose-6-phosphate (F6P) combining with ribose-5-phosphate (R5P) to form glycerdaldehyde-3-phosphate (GAP) and O8P, or from the dephosphorylation of octulose-1,8-bisphosphate (OBP), which is formed from dihydroxyacetone-phosphate (DHAP) combining with R5P (Clasquin, 2011). SBP may be synthesized from the phosphorylation of sedoheptulose-7-phosphate (S7P) or DHAP combining with erythrose-4-phosphate (E4P) (Clasquin, 2011). Fructose bisphosphate aldolase and sedoheptulose bisphosphatase were reported by Clasquin et al. to be involved in the formation of SBP and OBP in *Saccharomyces cerevisiae*. *P. putida* does contain fructose bisphosphate aldolase, responsible for converting DHAP and GAP to FBP, but sedoheptulose bisphosphatase has not yet been reported (PGD, 2014). Under (+)Fe growth conditions, SBP labeling matches the rate of S7P labeling (Figures 13 and 24A). O8P contains a high amount of 0-labeled carbons

after one hour, indicating a very small flux of carbon to this compound (Figure 24A). (-)Fe growth conditions saw the same trend for O8P labeling, that is mostly 0-labeled carbons remained after one hour (Figure 24A). SBP had a slower incorporation rate when Fe was limited. The trend of less fully labeled SBP than S7P under Fe-limited conditions indicates SBP is most likely being formed from S7P, but this conclusion is hard to support given that there is no distinct labeling pattern distinguishing either pathway as dominant (Figure 26).

In both Fe conditions for 1,2-^{13}C glucose kinetics, O8P contained more 2-labeled carbons than 1-labeled, which is most likely formed from 2-labeled F6P and 0-labeled R5P (Figure 24B). S7P can form three distinct ways (Figure 4): X5P combining with R5P to form GAP and S7P, F6P and E4P combining to form GAP and S7P, and the dephosphorylation of SBP (Clasquin, 2011). The presence of 1- and 2-labeled S7P can be explained by the labeling patterns of R5P, F6P and DHAP, all measurable metabolites. Figure 25 shows a schematic of the possible labeling combinations to get 2-labeled S7P. E4P cannot be measured via LC-MS, but is presumed to be 0-labeled based on its formation in the PP pathway (Figure 22). SBP contains mostly 0-labeled carbon, indicating the flux to this compound is relatively small in *P. putida* under (+) and (-)Fe conditions (Figure 25). To further support the presence of riboneogenesis in *P. putida*, genomics would be necessary to confirm the presence of sedoheptulose bisphosphatase and to confirm the role of fructose bisphosphate aldolase, in combining DHAP and E4P to make SBP, which was outside the scope of this project. The presence of these two compounds indicates the ability of *P. putida* to create energy storing compounds previously thought to be present in only photosynthetic organisms, and more recently yeasts (Clasquin, 2011). The comparable levels of labeling under each Fe condition suggest that limited Fe as an environmental stress does not affect their formation significantly.

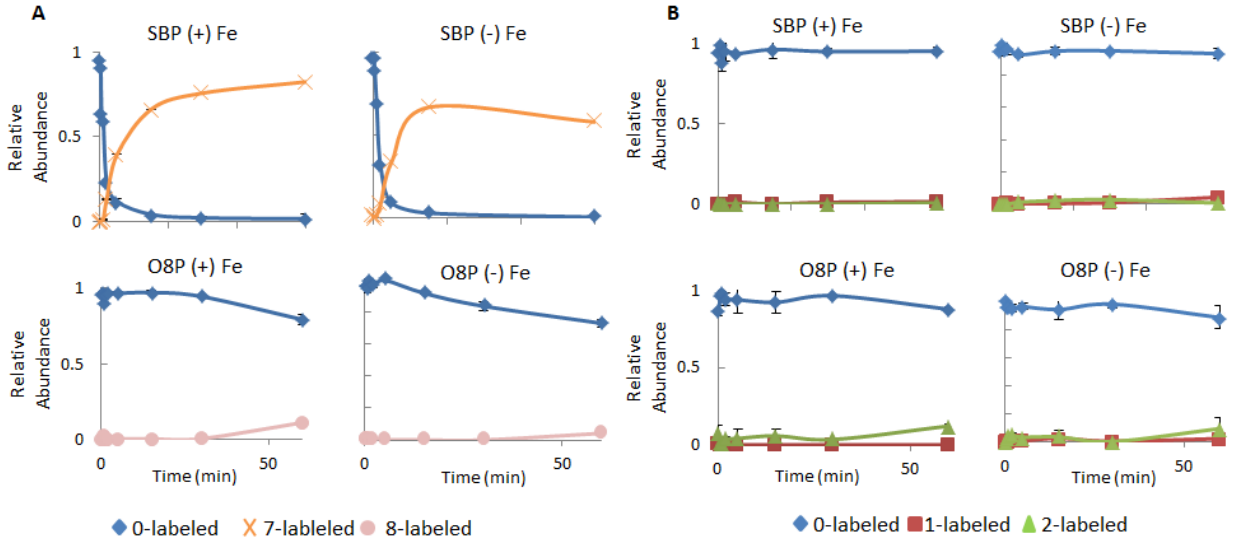

Figure 24. Kinetics for sedoheptulose-1,7-bisphosphate (SBP) and octulose-8-phosphate (O8P) under Fe-replete and Fe-limited conditions when grown on (A) [U-^{13}C] glucose or (B) [1,2-^{13}C] glucose. Values shown are averages of biological triplicates (A) or duplicates (B) with standard deviation error bars.

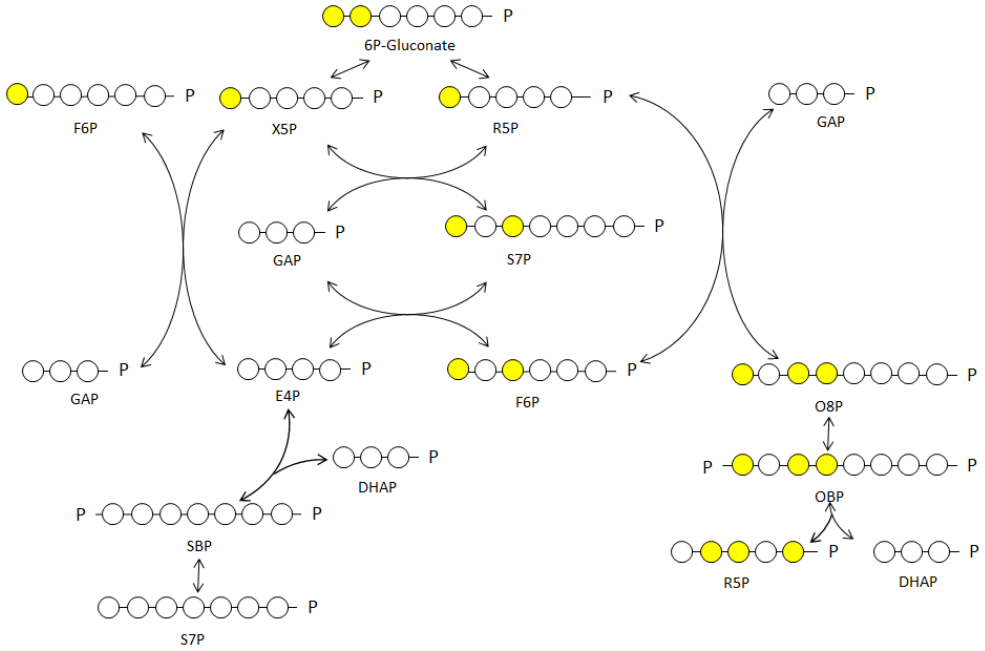

Figure 25. Labeling schematic of the pentose phosphate pathway with octulose-8-phosphate (O8P), sedoheptulose-1,7-phosphate (SBP) and octulose-1,8-bisphosphate (OBP) included for *P. putida* grown on [1,2-^{13}C] glucose. Yellow circles represent labeled carbons while white circles represent unlabeled carbons. Abbreviations are as follows: fructose-6-phosphate, F6P; xylulose-5-phosphate; ribose-5-phosphate, R5P; glyceraldehyde-3-phosphate, GAP; sedoheptulose-7-phosphate, S7P; erythrose-4-phsophate, E4P; octulose-8-phosphate, O8P; dihydroxyacetone phosphate, DHAP.

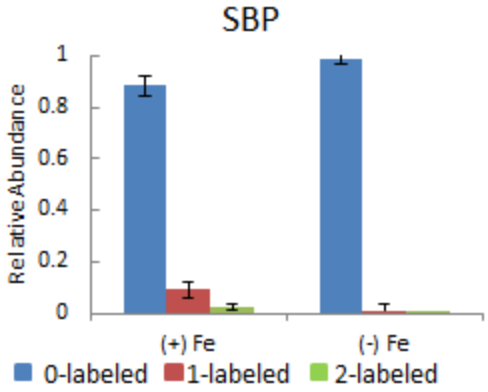

Figure 26. Relative abundance of steady-state labeling for sedoheptulose-1,7-bisphosphate (SBP) for *P. putida* grown on [1,2-^{13}C] glucose under Fe-replete and Fe-limited conditions. Values shown are averages of independent biological duplicates with standard deviation error bars.

Metabolic flux analysis for glucose grown cells

The labeling profiles gathered from the steady-state experiments were used as inputs in the metabolic flux model. To perform a complete mass balance on the central carbon metabolism of *P. putida*, excretion rates for extracellular metabolites and glucose consumption rates were needed. A number of metabolites were excreted under both Fe conditions (Table 3), but (-)Fe media contained more extracellular metabolites than (+)Fe media (11 and 9 metabolites, respectively; Table 3). Overall, (+)Fe *P. putida* excreted more glycolytic metabolites (mainly 3PG and pyruvate) while (-)Fe *P. putida* excreted more TCA cycle metabolites (mainly citrate, 2-ketoglutarate and malate; Table 3), which may be due to the insufficient expression of Fe-enzymes in the TCA cycle, as mentioned earlier. These results were consistent with the trend of more extracellular metabolites found in the early stationary growth phase of (-)Fe media (Table 2). Notably, excretion of gluconate was considerably higher in (-)Fe media (1780±370 µM/gCDW/hr) than (+)Fe media (157±23 µM/gCDW/hr; Table 3), which matched the high level of intracellular gluconate found in (-)Fe cells (Figure 10). Glucose is converted to gluconate and

2-ketogluconate in the periplasm before being transported inside the cell (del Castillo, 2007). Previously, *P. putida* was shown to release low levels of gluconate and 2-ketogluconate under Fe-replete conditions, but these metabolites were eventually consumed from the media (del Castillo, 2007). The uptake rates of glucose along with the growth constants for each condition were used to calculate efflux to biomass (Table 3); the uptake rates varied considerably from (+)Fe media (22.2±4.8 mM/gCDW/hr) to (-)Fe media (4.1±0.3 mM/gCDW/hr; Table 3).

The reaction network was compiled based on previously reported flux analysis of *P. putida* (del Castillo, 2007; Puchalka, 2008; Blank, 2008; Fuhrer, 2005). The model, in addition to estimating fluxes, also provided predictions for labeling profiles of the metabolites in the flux model which LC-MS data was provided as an input. A comparison between the experimentally determined steady-state labeling patterns and the predicted patterns serve as a way to validate the model; a good fit between the two patterns indicates an accurate prediction of flux values from the model. For both Fe conditions, the fit between the model predictions and experimentally determined labeling patterns matched well (Figures 27 and 28).

Fluxes to the PP pathway for both (+) and (-)Fe conditions were small (less than 5% of the uptake) compared to the fluxes through the rest of the central carbon metabolism (Figure 29). Puchalka et al. found the flux to the PP pathway was about 6% of the uptake rate, and the reactions in the PP pathway had flux values close to zero (Puchalka, 2008). Since almost half of the glucose taken up in (-)Fe media was excreted by the cell as gluconate (43.7%, Table 3), the resulting fluxes for (-)Fe condition should be at least half of those for (+)Fe. The ED pathway flux in (-)Fe was about half of that in (+)Fe (115.2±2.9 and 62.0±1.2, respectively), which follows the predicted trend. The flux from glucose to gluconate was higher under Fe-limited conditions, compared to Fe-replete conditions (93.3±3.1 and 61.3±0.1, respectively). The flux

from PEP to pyruvate was comparable in (-)Fe and (+)Fe conditions (62.1±15.1 and 64.9±0.9, respectively; Figure 29) and agreed with previously reported flux values (Puchalka, 2008; Sudarsan, 2014; Blank, 2008; Fuhrer, 2004). This corresponds to the high levels of intracellular pyruvate noted under (-)Fe conditions in Figure 10. As predicted with the steady state labeling of PEP, the flux from OAA to PEP was higher under (-)Fe than (+)Fe (21.3±14.1 and 9.5±0.0, respectively). The pyruvate shunt, which consists of the conversion from malate to pyruvate to OAA and is catalyzed by malic enzyme and pyruvate carboxylase, is favored over malate dehydrogenase (malate to OAA) under Fe-replete conditions (Fuhrer, 2005; Puchalka, 2008). This does not appear to be the favored route under Fe-limited conditions, where the pyruvate shunt and malate dehydrogenase reaction are close in magnitude (Figure 29). Overall, the fluxes between PEP, pyruvate and OAA appear to be elevated under Fe limited conditions, which may be due to the increased demand for amino acids to form pyoverdine.

The TCA cycle was less active when Fe was limited, which may be a function of the Fe-S containing TCA cycle enzymes, and may also explain why the glyoxylate shunt is active under Fe-limited conditions, but not Fe-replete conditions. The glyoxylate shunt has previously been shown to be inactive under Fe-replete conditions for glucose grown *P. putida* (Puchalka, 2008; Sudarsan, 2014; Fuhrer, 2004), and to be inactive in other bacteria species due to catabolite repression from glucose (Cozzone, 1998). The glyoxylate shunt bypasses both aconitase and succinate dehydrogenase, two Fe-S containing enzymes, to form malate, possibly making it a more favorable pathway to malate formation under Fe-limited conditions. It is interesting to note that the most dramatic decreases in flux occurred in the TCA cycle, which is mostly regulated by post-transcriptional and post-translational modifications, compared to the ED pathway which is transcriptionally regulated in *P. putida* (Sudarsan, 2014).

Table 3. Data used in metabolic flux analysis: excretion, growth, consumption, uptake and biomass conversion rates.

	Excretion rates (μM/gCDW/hr) ± standard deviation		
Metabolite	Glucose (+)Fe	Glucose (-)Fe	Succinate (+)Fe
3-phosphoglycerate	4.45±0.86	0±0	1.20±0.11
phosphoenolpyruvate	0.0040±0.0022	0±0	0.042±0.029
fumarate	0.039±0.013	0.0060±0.0006	1.09±0.32
malate	0.0078±0.0025	0.059±0.028	2.47±0.43
aspartate	0±0	0±0	0.30±0.02
ribose-5-phosphate	0.00649±0.0017	0.065±0.015	0.00156±0.00024
gluconate	157±23	1780±370	0±0
2-ketoglutarate	0±0	0.0302±0.044	0.61±0.19
glutamate	0±0	0.039±0.016	2.17±0.10
pyruvate	7.74±2.76	0.1130±0.0006	0.416±0.022
succinate	0±0	0±0	0±0
glucose-6-phosphate	0.0395±0.0033	0.0392±0.005	0.0066±0.0013
fructose-6-phosphate	0.0715±0.0095	0.083±0.012	0.019±0.004
6-phosphogluconate	0±0	0.19±0.15	0±0
citrate	0±0	7.85±3.48	0±0
	Growth and Consumption rates ± standard deviation		
growth rate (hr^{-1})	0.60±0.08	0.08±0.01	0.54±0.04
consumption rate (mM/OD)	12.90±0.68	18.54±0.05	11.11±0.67
uptake rate (mM/gCDW/hr)	22.2±4.8	4.08±0.33	17.1±5.5
	Biomass (μM/gCDW) ± standard deviation		
erythrose-4-phosphate	10.8±1.9	7.5±0.6	12.5±3.0
ribose-5-phosphate	7.4±1.3	5.18±0.4	8.6±2.1
3-phosphoglycerate	22.9±4.1	15.9±1.2	26.5±6.5
phosphoenolpyruvate	10.8±1.2	7.5±0.8	12.5±1.4
2-ketoglutarate	29.6±6.7	20.6±4.7	34.4±7.8
oxaloacetate	36.3±1.4	25.3±9.4	42.4±15.0
pyruvate	39.0±1.6	27.1±1.2	45.3±18.0

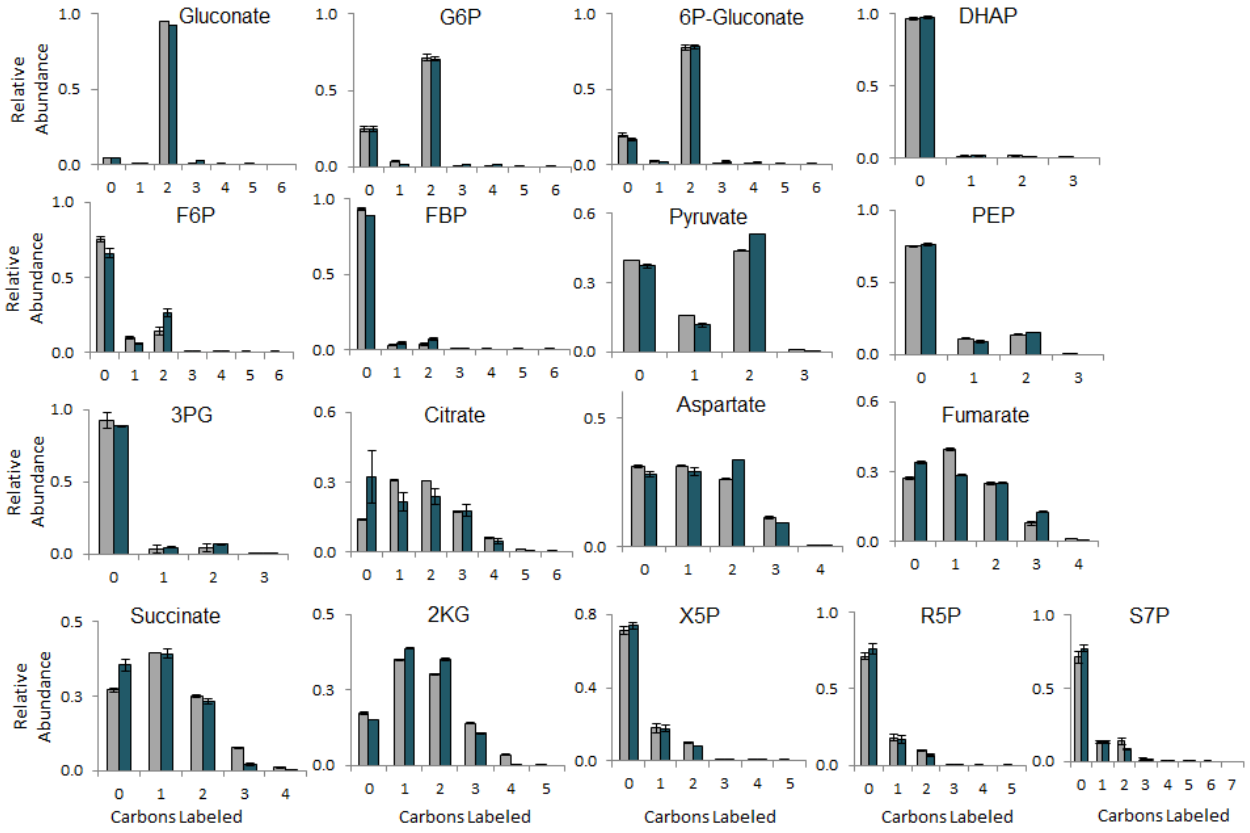

Figure 27. Model predictions (grey) of labeling abundances in the metabolites included in the flux model for glucose (+)Fe compared to the experimental LC-MS values at steady-state (blue). Data shown are averages of two model simulations and two replicate steady-state experiments with standard deviation error bars. Abbreviations are as follows: phosphoenolpyruvate, PEP; 3-phosphoglycerate, 3PG; 2-ketoglutarate, 2KG; fructose-1,6-bisphosphate, FBP; dihydroxyacetone phosphate, DHAP; fructose-6-phosphate, F6P; glucose-6-phosphate, G6P; sedoheptulose-7-phosphate, S7P; ribose-5-phosphate; xylulose-5-phosphate.

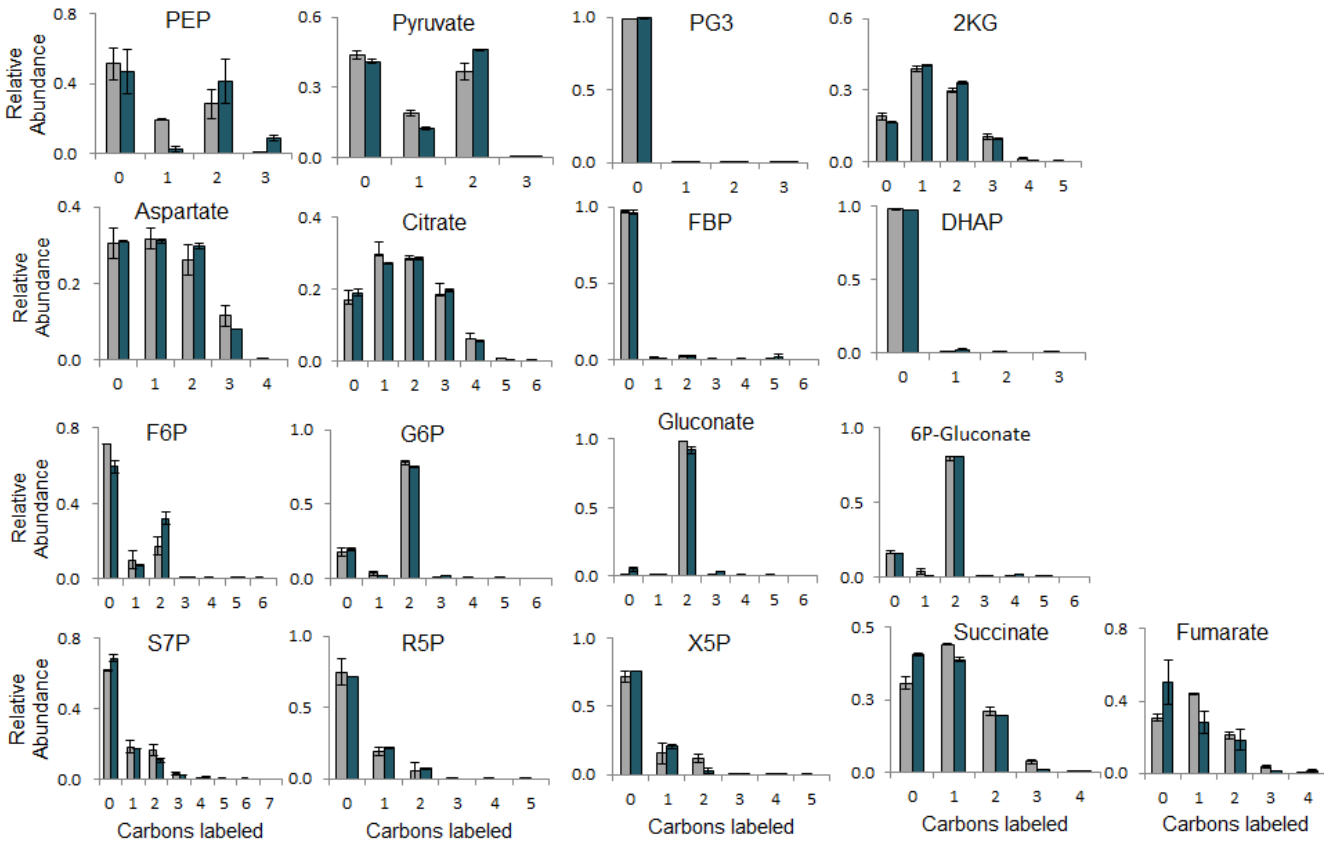

Figure 28. Model predictions (grey) of labeling abundances in the metabolites included in the flux model for glucose (-)Fe compared to the experimental LC-MS values at steady-state (blue). Data shown are averages of two model simulations and two replicate steady-state experiments with standard deviation error bars. Abbreviations are as follows: phosphoenolpyruvate, PEP; 3-phosphoglycerate, 3PG; 2-ketoglutarate, 2KG; fructose-1,6-bisphosphate, FBP; dihydroxyacetone phosphate, DHAP; fructose-6-phosphate, F6P; glucose-6-phosphate, G6P; sedoheptulose-7-phosphate, S7P; ribose-5-phosphate; xylulose-5-phosphate.

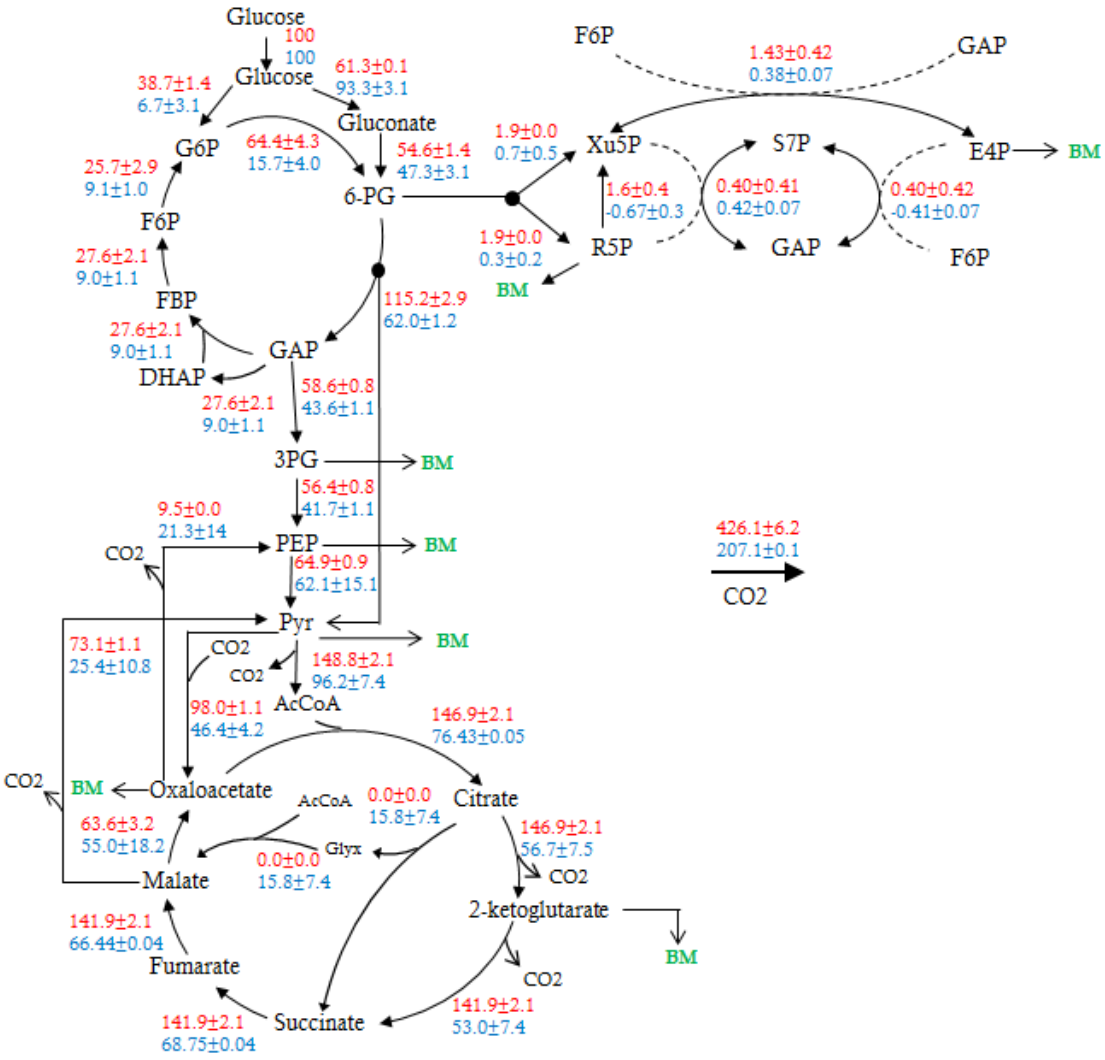

Figure 29. Comparison of fluxes between (+)Fe (red) and (-)Fe (blue) growth conditions. Values shown are averages between two biological replicates ± standard error and are normalized to the uptake rate, set to 100. Dashed lines in the pentose phosphate pathway indicate reversible reactions. Reversible reactions in glycolysis or the TCA cycle are not marked; arrows simply indicate the direction of flux. Fluxes are a fraction of the uptake rate (set to 100) and biomass (BM) and excretion rates are fractions of the uptake rate, with actual values reported in Table 3.

Additionally, the model was able to predict carbon dioxide flux, calculated by summing all CO_2 producing reactions (Table 4). Not surprisingly, glucose consumption under Fe-replete conditions produced more CO_2 (94.75±1.38 mM/gCDW/hr) than under Fe-limited conditions (8.45±0.10 mM/gCDW/hr; Table 4), but the CO_2 released under Fe-limited conditions is nearly

proportional to the difference in uptake rates between the two Fe conditions (Table 3). The smaller carbon dioxide flux is a function of decreased uptake when Fe is limited (Table 3), decreased flux to CO_2 producing TCA cycle reactions, and the excretion of a large portion of glucose through gluconate, preventing it from being metabolized further. Carbon dioxide produced from soil respiration is a large terrestrial source of carbon into the atmosphere, estimated at $7.5x10^{15}$ g C/yr (Schlesinger, 2000; Sullivan, 2008). Increasing temperatures are expected to affect microbial respiration in soils, and thus the efflux of CO_2 to the atmosphere, but available organic substrates and other environmental stresses, like nutrient availability, will also affect respiration and CO_2 flux.

Table 4. CO_2 generated from flux models (mM/gCDW/hr) with standard deviation

Glucose (+)Fe	Glucose (-)Fe	Succinate (+)Fe
94.75±1.38	8.45±0.10	10.44±0.46

The results presented in this section highlight the importance of MFA in understanding the adaptability of bacterial metabolisms to different environmental stresses and the mechanisms which regulate metabolism by routing carbon towards relevant biomass precursors. MFA also serves as a useful complementary tool to transcriptomics and genomics which cannot convey the changes in metabolite fluxes in pathways that are not directly regulated by genes. The results presented in this section demonstrate the robustness of *P. putida* under Fe stress. *P. putida* is able to reroute carbon under Fe-limited conditions to amino acid precursors, like PEP, while maintaining fluxes in central carbon metabolic pathways. Understanding the adaptability of *P. putida* to different environmental stresses is important for its use in biotechnological applications as a means to produce biofuels and chemicals, in addition to environmental engineering applications such as bioremediation of contaminated soils.

CHAPTER 5

METABOLISM OF SUCCINATE

To compare central carbon metabolic fluxes across different substrates, [2,3-^{13}C] succinate incorporation into the TCA cycle was investigated. Succinate is one of the most common root exudates found in soils (Lipton, 1987), and its incorporation into the central carbon metabolism in *P. putida* has not been extensively studied. Excretion rates were first measured in early exponential phase to account for carbon flux out of *P. putida* cells (Table 3). Higher levels of TCA cycle intermediates were secreted on (+)Fe succinate grown bacteria compared to (+)Fe and (-)Fe glucose grown bacteria (Table 3), mainly fumarate, malate, aspartate, glutamate, and 2-ketoglutarate. Other metabolites from glycolysis and the PP pathway were comparable or lower than (+)Fe glucose grown bacteria (Table 3). Higher amounts of excreted TCA cycle compounds were mentioned previously in Chapter 2 and were hypothesized to be a result of overflow metabolism.

The steady-state labeling patterns for TCA cycle intermediates (Figure 30) showed consistent labeling patterns in succinate, fumarate and malate, all containing mostly (more than 80%) 2-labeled carbons. Aspartate contained mostly 2-labeled carbon (more than 60%), but contained more 4-labeled carbons (more than 20%) than malate (5 %). If aspartate was formed primarily via the malate dehydrogenase route, there would be less 4-labeled and more 2-labled aspartate. Additionally, if the TCA cycle were making more complete turns, there would be an enrichment in 4-labeled succinate, fumarate and malate (Figure 31A), but the elevation of 2-labeled carbons in these metabolites suggest this is not occurring. The glyoxylate shunt appears to be active (Figure 31B), which would produce mostly 3-labeled malate and succinate, and

subsequently 3-labeled aspartate. There is 4% 3-labeled malate, 10% 3-labeled aspartate, but 0% 3-labeled succinate. One explanation to the surprisingly lack of 3- and 4-labeled succinate is that the labeling may be skewed due to the rapid uptake of [2,3-^{13}C] succinate (17.1±5.5 mM/gCDW/hr; Table 3), essentially saturating the pool of intracellular metabolites close to succinate. For this reason, succinate labeling was not included in the succinate flux model.

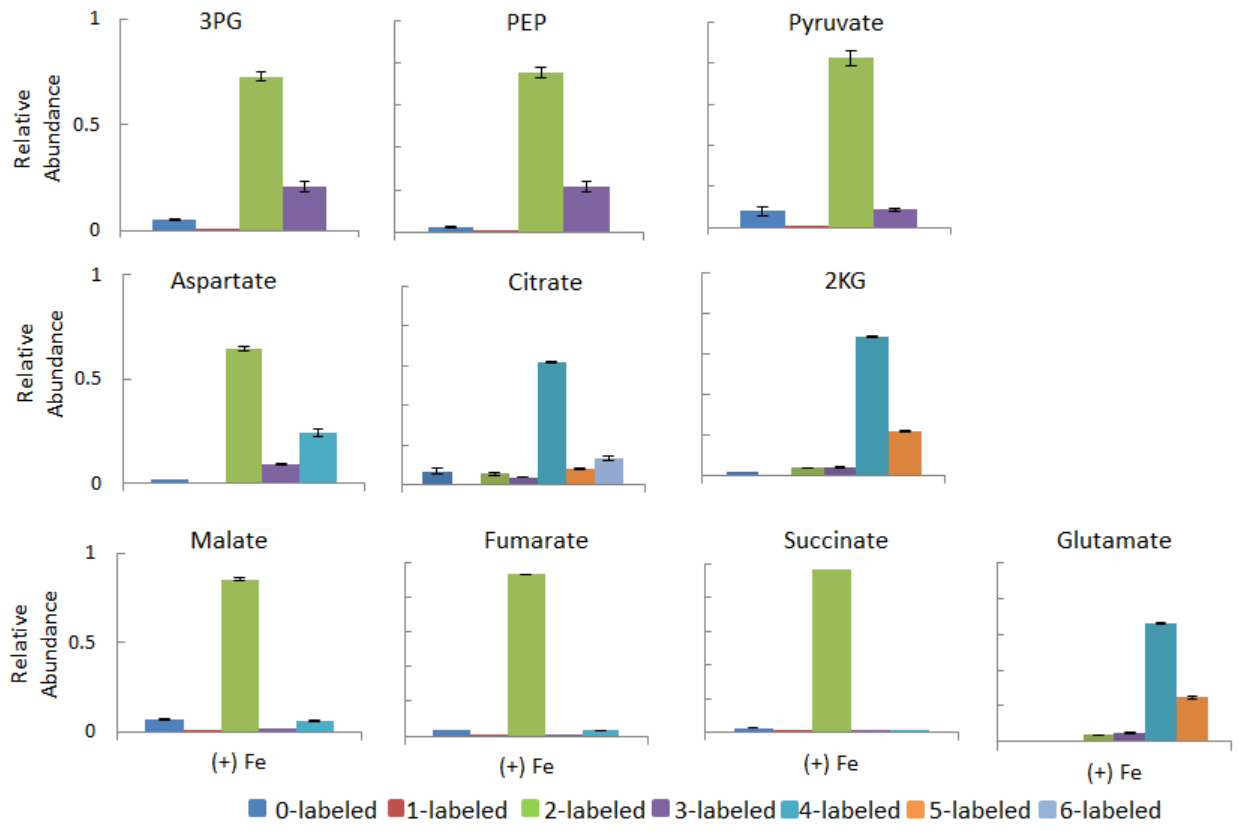

Figure 30. Steady state labeling data for TCA cycle intermediates for *P. putida* grown on [2,3-^{13}C] succinate. Samples are averages with standard deviation error bars (n=2). Abbreviations are as follows: 3-phosphoglycerate, 3PG; phosphoenolpyruvate, PEP; 2-ketoglutarate, 2KG.

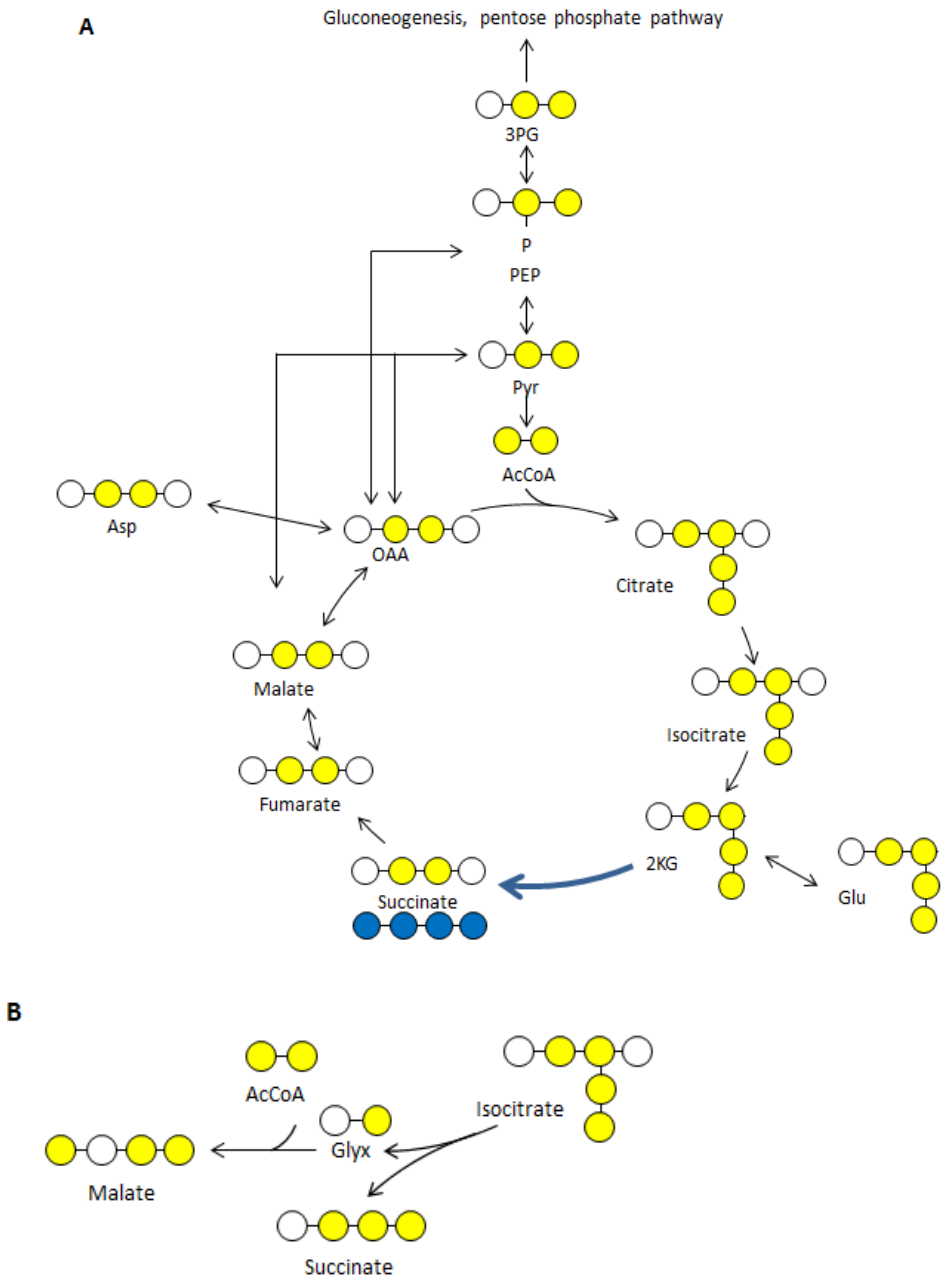

Figure 31. Labeling pattern schematic the TCA cycle of *P. putida* grown on [2,3-^{13}C] succinate. The TCA cycle and the first two reactions of gluconeogenesis are shown in (A) while (B) shows the glyoxylate shunt of the TCA cycle. Yellow and blue circles represent labeled carbons. Yellow circles represent one round of the TCA cycle, beginning with succinate and ending with 2-ketoglutarate. The blue circles represent the labeling of succinate at the beginning of a second round of the TCA cycle. Abbreviations are as follows: 3-phosphoglycerate, 3PG; phosphoenolpyruvate, PEP; pyruvate, pyr; acetyl-CoA, AcCoA; oxaloacetate, OAA; 2-ketoglutarate, 2KG; glutamate, glu; glyoxylate, glyx; aspartate, asp.

The labeling patterns predicted by the succinate flux model match with the experimental carbon labeling patterns (Figure 32). The match between the two patterns indicates the fluxes predicted from the model are of good quality. The flux model for succinate shown in Figure 33 reveals a decreased flux from OAA and acetyl-CoA to citrate, citrate to 2-ketoglutarate, and 2-ketoglutarate to succinate (29.0±1.2, 26.2±0.8, and 19.0±1.0, respectively), compared to the high flux from succinate to fumarate, and fumarate to malate (121.8±4.8, 121.0±4.9, respectively). In contrast to the favored pyruvate shunt found with (+)Fe and (-)Fe growth on glucose, (+)Fe succinate metabolism favors the malate dehydrogenase reaction (Figure 33). Additionally more OAA is routed to pyruvate than PEP, which is in agreement with the fluxes reported by Sudarsan et al. of benzoate grown *P. putida* (Sudarsan, 2014). Benzoate is split into acetyl-CoA and succinate, so it is likely the metabolism of succinate would follow that of benzoate. Sudarsan et al. also reported the glyoxylate shunt to be very active, routing four times more carbon than the flux from citrate to 2-ketoglutarate to succinate (Sudarsan, 2014). The model presented here determined the glyoxylate shunt to have a flux of 2.8±0.4 (Figure 33), which is in contrast to the inactive glyoxylate shunt from the (+)Fe glucose model. Catabolite repression does not occur when *P. putida* grows on TCA cycle intermediates like succinate and acetate (Cozzone, 1998). Sudarsan et al. reported a high glyoxylate shunt flux, equivalent to the uptake rate of benzoate; the discrepancy between this reported flux and the flux determined by the succinate model can be partially explained by benzoate splitting into equal amounts of acetyl-CoA and succinate, both of which are routed toward the glyoxylate shunt (Sudarsan, 2014). The labeling data presented in Figure 30 do not support a highly active glyoxylate shunt, so the discrepancy cannot be completely resolved.

The carbon dioxide flux from the succinate (+)Fe model was determined to be 10.44±0.46 mM/gCDW/hr (Table 4). This is comparable to the CO_2 released in the (-) Fe glucose model, and less than half of the CO_2 release in the (+)Fe glucose model (Table 4). The lower carbon dioxide flux from the succinate model is a result of the decreased flux of the CO_2 generating reactions of the TCA cycle (citrate to 2-ketoglutarate, 2-ketoglutarate to succinate), and the smaller flux of pyruvate to acetyl-CoA (Figure 33). This indicates that *P. putida* releases less carbon dioxide, and conserves more carbon converting substrate to biomass when grown on succinate compared to glucose, which is a significant finding consider succinate is a preferred substrate to glucose.

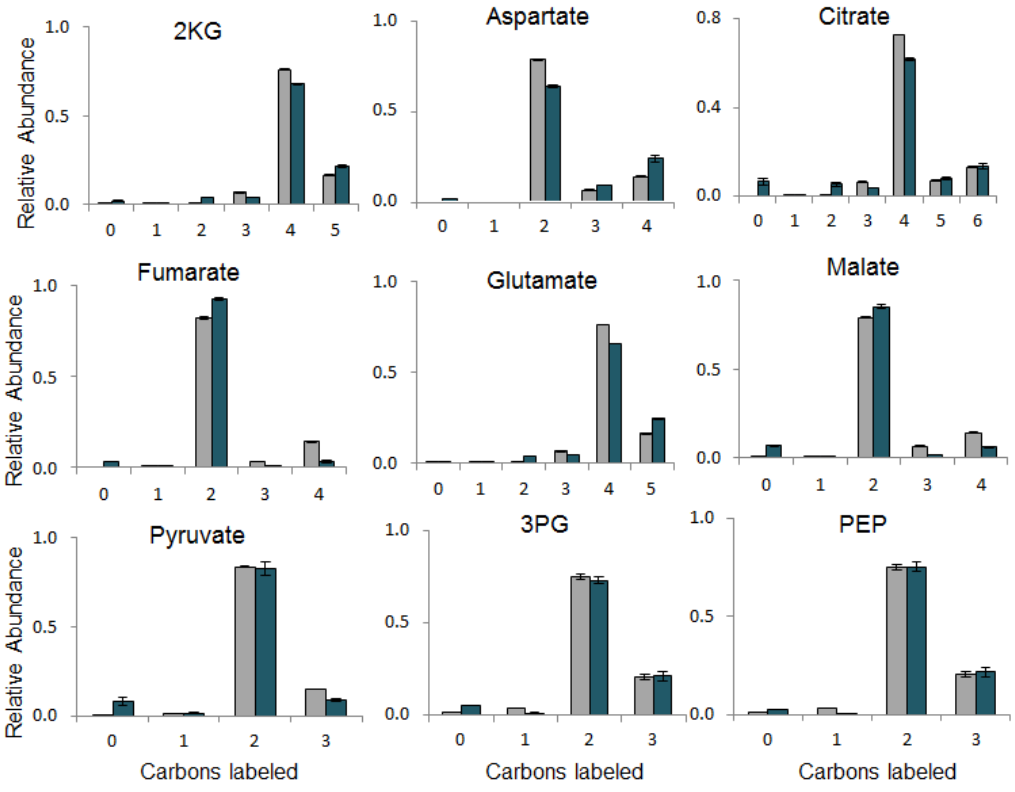

Figure 32. Model predictions (grey) of labeling abundances in the metabolites included in the flux model for succinate (+)Fe compared to the experimental LCMS values at steady-state (blue). Data shown are averages of two model simulations or two replicate steady-state experiments with standard deviation error bars. Abbreviations are as follows: 2-ketoglutarate, 2KG; 3-phosphoglycerate, 3PG; phosphoenolpyruvate, PEP.

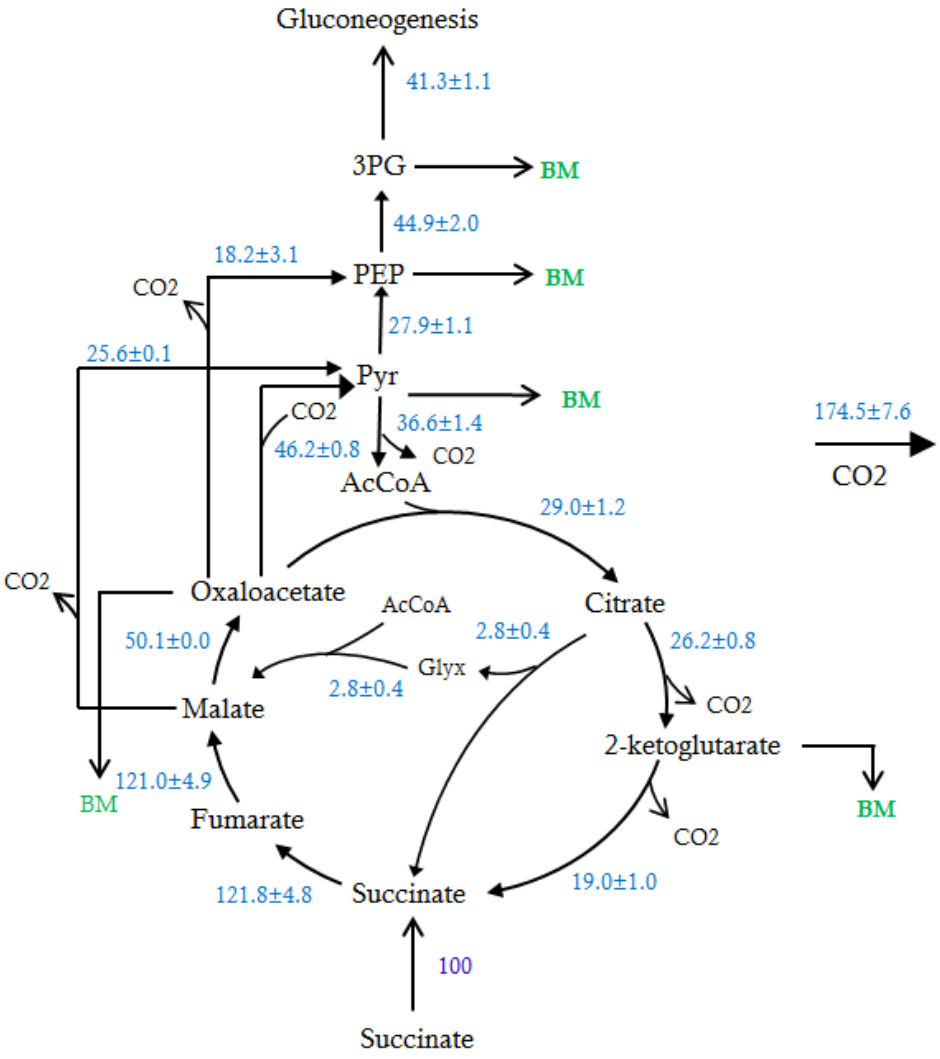

Figure 33. Flux of succinate through the TCA cycle under (+)Fe conditions. Flux values (in blue) are averages of two biological replicates with standard error. Flux values are normalized to the uptake rates (set to 100). Compounds that are precursors to biomass are marked (BM). Abbreviations are as follows: 3-phosphoglycerate, 3PG; phosphoenolpyruvate, PEP; pyruvate, Pyr; acetyl-CoA, AcCoA; glyoxylate, glyx.

It is important to compare fluxes of carbon substrates with different entry points in the carbon metabolism. As hypothesized earlier, the metabolism of substrates with different entry points in the carbon metabolism results in different metabolite excretions. Carbon fluxes in the central carbon metabolic pathways change based on the entry point of growth substrates, typically experiencing higher fluxes closer to the point of entry. This was observed in the

excretion rates at stationary phase on all four growth substrates (glucose, citrate, succinate, and acetate) and was also detected at early exponential phase between Fe-replete glucose and succinate grown *P. putida*. Elucidating the intracellular carbon flux as a response to succinate uptake is an important contribution to understanding the versatility of *P. putida*'s metabolism.

CHAPTER 6

FUTURE DIRECTIONS

P. putida is noted for having a resilient and versatile metabolism. This research presented a flux analysis of two separate carbon sources. Flux analyses of mixed carbon substrates have not yet been performed, modeling the simultaneous incorporation of glucose and succinate into the central carbon metabolism would provide more insights into the metabolism of *P. putida* in environmental soil conditions. Additionally, since the response of Pseudomonad metabolism to Fe stress has not been well studied, there are a number of follow up experiments to the work presented in here that would contribute to this topic. Concentrations of key intracellular metabolites were presented in Chapter 2, but monitoring the change in the entire intracellular metabolome under Fe-replete and Fe-limited conditions would provide a complete picture of the enrichment or depletion of intracellular metabolites. Additionally, quantifying levels of intracellular amino acids would provide a better understanding of the amino acids affected under Fe-limited conditions (Shakoury-Elizeh, 2010) and may reveal trends in the pooling of certain amino acids to form pyoverdine. One question raised by the flux modeling of different Fe conditions was why gluconate excretion levels were so much higher in (-) Fe-grown glucose conditions. This increased excretion may be caused by direct or indirect regulation of gluconokinase or the gluconate transporter by Fe. Transcriptomic analysis would be necessary to elucidate the cause of gluconate pooling and excretion under Fe-limited conditions. Although, it is important to note that many of the reactions in the central carbon metabolism of *P. putida* are not transcriptionally regulated, but may be controlled by post-translational mechanisms or allosteric inhibition (Sudarsan, 2014).

Two untargeted compounds, O8P and SBP, previously thought to only exist in photosynthetic organisms were found in the intracellular media of *P. putida* when grown on glucose. To determine if the pathways forming these compounds are similar to the yeast *S. cerevisaea* genomics would be necessary to test for the two enzymes (sedoheptulose bisphosphatase and fructose bisphosphate aldolase) responsible for their anabolic pathways (Clasquin, 2011). Additional labeling experiments with [1-^{13}C] or [1,6-^{13}C] labeled glucose could provide distinct labeling patterns to determine which formation pathway is favored. This would also allow the central carbon metabolism flux model presented in the previous section to be expanded, providing a more accurate representation of carbon routing in *P. putida*

BIBLIOGRAPHY

Albrecht-Gary, A.-M.; Blanc, S.; Rochel, N.; Ocaktan, A. Z.; Abdallah, M. A., Bacterial Iron Transport: Coordination Properties of Pyoverdin PaA, a Peptidic Siderophore of Pseudomonas aeruginosa. *Inorganic Chemistry* 1994**.** 33(26): 6391-6402.

Amador-Noguez, D.; Feng, X.J.; Fan, J.; Roquet, N.; Rabitz, H.; Rabinowitz, J. D. Systems-level metabolic flux profiling elucidates a complete, bifurcated tricarboxylic acid cycle in Clostridium acetobutylicum. 2010. *J. Bacteriol*. 192(17).

Andrews, S. C.; Robinson, A. K.; Rodriguez-Quinones, F., Bacterial iron homeostasis. *Fems Micriobio Reviews*. 2003. 27(2-3):215-237.

Antoniewicz, M. R., 13C metabolic flux analysis: optimal design of isotopic labeling experiments. 2013. *Current Opinion in Biotechnology*. 24(6):1116-1121.

Archibald, F. S.; DeVoe, I. W., Iron acquisition by Neisseria meningitidis in vitro. *Infection and Immunity* 1980**.** 27(2): 322-334.

Aristilde, L.; Xu, Y.; Morel, F. M. M., Weak Organic Ligands Enhance Zinc Uptake in Marine Phytoplankton. *Environmental Science & Technology* 2012**.** 46(10): 5438-5445.

Asai, T.; Aida, K.; Sugisaki, Z.; Yakeishi, N., On a-ketoglutaratic acid fermentation. *J Gen. Appl. Microbiol.*1995. 1:308-346.

Badri, D. V.; Vivanco, J. M., Regulation and function of root exudates. *Plant Cell Environ.* 2009. 32(6): 666-681.

Blank, L.; Ionidis, G.; Ebert, B.; Buhler, B.; Schmid, A., Metabolic response of Pseudomonas putida during redox biocatalysis in the presence of a second octanol phase. *FEBS Jour*. 2008. 275:5173-5190.

Bi, Y; Hesterberg, D. L.; Duckworth, O. W., Siderophore-promoted dissolution of cobalt from hydroxide minerals. *Geochimica et Cosmochimica Acta*. 2010. 74(10): 2915-2925.

Bultreys, A.; Gheysen, I., Production and Comparison of Peptide Siderophores from Strains of Distantly Related Pathovars of Pseudomonas syringae and Pseudomonas viridiflava LMG 2352. *Applied and Environmental Microbiology* 2000. 66(1): 325-331.

Castillo, T.; Ramos, J.; Rodriguez-Herva, J.; Fuhrer, T.; Sauer, U.; Duque, E., Convergent peripheral pathways catalyze initial glucose catabolism in Pseudomonas putida: genomic and flux analysis. *J Bacteriol*. 2007. 189(14):5142-5152.

Chavarria, M.; Nikel, P. I.; Perez-Pantoja, D.; de Lorenzo, V. The entner-doudoroff pathway empowers Pseudomonas putida KT2440 with a high tolerance to oxidative stress. *Environ Microbiol*. 2012. 15(6): 1772-1785.

Cheah, S. F.; Kraemer, S. M.; Cervini-Silva, J.; Sposito, G., Steady-state dissolution kinetics of goethite in the presence of desferrioxamine B and oxalate ligands: implications for the microbial acquisition of iron. *Chemical Geology*. 2003. 198(1-2):63-75.

Clasquin, M. F.; Melamud, E.; Singer, A.; Gooding, J. R.; Xu, X.; Dong, A.; Cui, H.; Campagna, S. R.; Savchenko, A.; Yakunin, A. F.; Rabinowitz, J. D.; Caudy, A. A.. Riboneogenesis in yeast. *Cell* 2011. 145:969-980.

Cornelis, P., Iron uptake and metabolism in pseudomonads. *Applied microbiology and biotechnology* 2010. 86(6): 1637-1645.

Cornish-Bowden, A., Biochemistry: Curbing the excesses of low demand. *Nature* 2013. 500(7461), 157-158.

Cozzone, A. J., Regulation of acetate metabolism by protein phosphorylation in enteric bacteria. *Ann Rev Microbiol*. 1998. 52:127-164.

del Castillo, T.; Ramos, J. L.; Rodríguez-Herva, J. J.; Fuhrer, T.; Sauer, U.; Duque, E., Convergent Peripheral Pathways Catalyze Initial Glucose Catabolism in Pseudomonas putida: Genomic and Flux Analysis. *Journal of Bacteriology* 2007. 189(14), 5142-5152.

Crown, S. B.; Antoniewicz, M. R., Parallel labeling experiments and metabolic flux analysis: past, present and future methodologies. *Metaboli Engineering*. 2012. 16:21-32.

Dinkla, I. J. T.; Janssen, D. B., Simulataneous growth on citrate reduces the effects of iron limitation during toluene degradation in Pseudmonas. *Microb. Ecology*. 2003. 45(1):97-107.

Duckworth, O. W.; Martin, S. T., Surface complexation and dissolution of hematite by C1-C6 dicarboxylic acids at pH = 5.0. *Geochimica et Cosmochimica Acta* 2001. 65(23), 4289-4301.

Duckworth, O. W.; Sposito, G., Siderophore-manganese (III) interactions. I. Air-oxidation of manganese(II) promoted by desferrioxamine B. *Environmental Science and Technology*. 2005. 39(16) 6037-6044.

Duckworth, O. W.; Holmström, S. J. M.; Peña, J.; Sposito, G., Biogeochemistry of iron oxidation in a circumneutral freshwater habitat. *Chemical Geology* 2009. 260(3–4), 149-158.

Duffy, B. K.; Défago, G., Environmental Factors Modulating Antibiotic and Siderophore Biosynthesis by Pseudomonas fluorescensBiocontrol Strains. *Applied and Environmental Microbiology* 1999. 65(6), 2429-2438.

Ebert, B. E.; Kurth, F.; Grund, M.; Blank, L. M.; Schmid, A., Response of Pseudomonas putida KT2440 to increased NADH and ATP demand. *Appl Environ Microbiol*. 2011. 77:6597-6605.

Evers, A.; Hancock, R. D.; Martell, A. E.; Motekaitis, R. J., Metal ion recognition in ligands with negatively charged oxygen donor groups. Complexation of iron (III), gallium (III), indium (III), aluminum (III), and other highly charged metal ions. *Inorganic Chemistry*. 1989. 28(11):2189-2195.

Filiatrault, M. J.; Stodghill, P. V.; Bronstein, P. A.; Moll, S.; Lindeberg, M.; Grills, G.; Schweitzer, P.; Wang, W.; Schroth, G. P.; Luo, S.; Khrebtukova, I.; Yang, Y.; Thannhauser, T.; Butcher, B. G.; Cartinhour, S.; Schneider, D. J. Trascriptome analysis of Pseudomonas syringae identifies new genes, noncoding RNAs, and antisense activity. 2010. 192(9):2359-2374.

Folsom, J. P.; Parker, A. E.; Carlson, R. P., Physiological and proteomic analysis of Escherichia coli iron-limited chemostat growth. *Journal of Bacteriology*. 2014. 196(15):2748.

Fuhrer, T.; Fischer, E.; Sauer, U., Experimental identification and quantification of glucose metabolism in seven bacterial species. *J Bacteriol*. 2005. 187(5):1581-1590.

Goyne, K. W.; Brantley, S. L.; Chorover, J., Effects of organic acids and dissolved oxygen on apatite and chalcopyrite dissolution : implications for using elements as organomarkers and oxymarkers. *Chemical Geology*. 2006. 234(1-2): 28-45.

Han, K.; Lim, H. C.; Hong, J., Acetic acid formation in escherichia coli fermentation. *Biotechnology and Bioengineering* 1992. 39(6), 663-671.

Harding, R. A.; Royt, P. W., Acquisition of iron from citrate by Pseudomonas aeruginosa. *Journal of General Microbiology* 1990. 136(9), 1859-1867.

Hemlem, B. J.; Vane, L. M.; Sayles, G. D., Stability constants for complexes of the siderophore desferrioxamine B with selected heavy metal cations. *Inorganica Chimica Acta*. 1996. 244(2):179-184.

Hider, R.; Kong, X., Chemistry and biology of siderophores. *Natural product reports.* 2010. 27(5):637-657.

Hinteregger, C.; Leitner, R.; Loidl, M.; Ferschl, A.; Streichsbier, F., Degradation of phenol and phenolic compounds by Pseudomonas putida EKII. *Applied Microbial and Biotechnology*.1992. 37:252-259.

Illmer, P.; Schinner, F., Solubilization of inorganic phosphates by microorganisms isolated from forest soils. *Soil Biology and Biochemistry* 1992. 24(4):389-395.

Kim, B. J.; Park, J. H.; Park, T. H.; Bronstein, P. A.; Schneider, D. J.; Cartinhour, S. W.; Shuler, M. L., Effect of iron concentration on the growth rate of Pseudomonas syringae and the expression of virulence factors in hrp-inducing minimal medium. *Appl. Env. Microbio.* 2009. 75(9):2720-2726.

Kraemer, S. M.; Crowley, D. E.; Kretzschmar, R., Geochemical aspects of phytosiderophore-promoted iron acquisition by plants. *Advances in Agronomy*. 2006. 91:1-46.

Kremling, A.; Pfluger-Grau, K.; Chavarria, M.; Puchalka, J.; dos Santos, V. M.; de Lorenzo, V., Modeling and analysis of flux distributions in the two branches of the phosphotransferase system in Pseudomonas putida. *BMC Systems Biology*. 2012. 6:149.

Koepsell, H. J.; Stodola, F. H.; Sharpe, E. S., Production of a-ketoglutarate in glucose oxidation by Pseudomonas fluorescens. *J. Am. Chem. Soc.* 1952. 74:5142-5144.

Lamont, I.; Martin, L. W., Identification and characterization of novel pyoverdine synthesis genes in Pseudomonas aeruginosa. *Microbiol.* 2003.149:833-842.

Lessie, T. G.; Phibbs, P. V., Jr. Alternative pathways of carbohydrate utilization in pseudomonads. *Annu Rev. Microbiol.* 1984. 38:359-388.

Lewis, K. F.; Blumenthal, H. J.; Weinrach, R. S.; Weinhouse, S., An isotope tracer study of glucose catabolism in Pseudomonas fluorescens. *J Biol Chem*. 1955. 216:273-286.

Li, H.; Xu, X.; Chen, H.; Zhang, Y.; Xu, J.; Wang, J.; Lu, X., Molecular analyses of the functional microbial community in composting by PCR-DGGE targeting the genes of the beta-glucosidase. *Bioresourse Technology*. 2013. 134:51-58.

Lim, C. K.; Hassan, K. A.; Tetu, S. G.; Loper, J. E.; Paulsen, I. T., The effect of iron limitation on the transcriptome and proteome of Pseudomonas fluorescens Pf-5. *PLOS ONE*. 2012. 7(6).

Lindsay, W. L.; Schwab, A. P., The chemistry of iron in soils and its availability to plants. *J Plant Nutrition*. 1982. 5(4-7):821-840.

Lipton, D. S.; Blanchar, R. W.; Blevins, D. G., Citrate, malate, and succinate concentration in exudates from p-sufficient and p-stressed *Medicago sativa* L. seedlings. *Plant Physiol*. 1987. 85: 315-317.

Marshall, B.; Stintzi, A.; Gilmour, C.; Meyer, J.-M.; Poole, K., Citrate-mediated iron uptake in Pseudomonas aeruginosa: involvement of the citrate-inducible FecA receptor and the FeoB ferrous iron transporter. *Microbiology* 2009. 155(1), 305-315.

Mansour, H. B.; Dellai, A.; Ayed, Y., Toxicities effects of pharmaceutical, olive mill and textile wastewaters before and after degradation by Pseudomonas putida mt-2. *Cancer cell international*. 2012. 21(2):136-138.

Mansour, H. B.; Mosrati, R.; Barillier, D.; Ghedira, K.; Chekir-Ghedira, L., Bioremediation of industrial pharmaceutical drugs. *Drug and Chemical Toxicology*. 2012. 35(3): 235-240.

Mapelli, V.; Olsson, L.; Nielsen, J. Metabolic footprinting in microbiology: methods and applications in functional genomics and biotechnology. *Trends in Biotechnology*. 2008. 26(9):490-497.

Meyer, J.-M.; Gruffaz, C.; Raharinosy, V.; Bezverbnaya, I.; Schafer, M.; Budzikiewicz, H., Siderotyping of fluorescent Pseudomonas: molecular mass determination by mass spectrometry as a powerful pyoverdine siderotyping method. *Biometals*. 2008. 21(3): 259-271.

Meyer, J.-M.. Pyoverdines: pigments, siderophores and potential taxonomic markers of fluorescent *Pseudomonas* species. *Arch Microbiol.* 2000. 174:135-142.

Meyer, J.-M.; Hornsperger, J. M., Role of pyoverdinepf, the iron-binding fluorescent pigment of Pseudomonas fluorescens, in iron transport. *J Gen Microbiol*. 1978. 107:329-331.

Meyer, J.-M.; Abdallah, M. A., The fluorescent pigment of Pseudomonas fluorescens: biosynthesis, purification and physicochemical properties. *J Gen Microbiol.* 1978. 107:319-328.

Molina, L.; Ramos, C.; Duque, E.; Ronchel, M. C.; Garcia, J. M.; Wyke, L.; Ramos, J. L., Survival of Pseudomonas putida KT2440 in soil and in the rhizosphere of plants under greenhouse and environmental conditions. *Soil Biology and Biochemistry*. 2000. 32(3): 315-321.

Nigam, A.; Phale, P. S.; Wangikar, P., Assessment of the metabolic capacity and adaptability of aromatic hydrocarbon degrading strain Pseudomonas putida CSV86 in aerobic chemostat culture. *Bioresource Technology*. 2012. 114: 484-491.

Otto, C.; Yovkova, V.; Barth, G., Overproduction and secretion of α-ketoglutaric acid by microorganisms. *Applied microbiology and biotechnology* 2011. 92(4): 689-695.

Pfluger, K.; de Lorenzo, V., Evidence of in vivo cross talk between the nitrogen-related and fructose-related branches of the carbohydrate phosphotransferase system of Pseudomonas putida. *J Bacteriol*. 2008. 190(9):3374.

PGD. "Pseudomonas Genome Database." www.pseudomonas.com

Philpott, C. C.; Leidgens, S.; Frey, A. G., Metabolic remodeling in iron-deficient fungi. *Biochimica et Biophysica Acta*. 2012. 1823:1509-1520.

Poblete-Castro, I.; Becker, J.; Dohnt, K.; dos Santos, V. M.; Wittmann, C., Industrial biotechnology of Pseudomonas putida and relate species. *Appl Micribiol Biotechnol*. 2012. 93:2279-2290.

Puchalka, J.; Oberhardt, M. A.; Godinho, M.; Bielecka, A.; Regehnardt, D.; Timmis, K. N.; Papin, J. A.; Martins dos Santos, V. A. P. Genome-scale reconstruction and analysis of the Pseudmonas putida KT2440 metabolic network facilitates applications in biotechnology. *PLOS Computational Biology*. 2008. 4(10).

Ravel, J.; Cornelis, P., Genomics of pyoverdine-mediated iron uptake in pseudomonads. *Trends in Microbiology* 2003. 11(5), 195-200.

Reaves, M. L.; Young, B. D.; Hosios, A. M.; Xu, Y.-F.; Rabinowitz, J. D., Pyrimidine homeostasis is accomplished by directed overflow metabolism. *Nature* 2013. 500(7461), 237-241.

Reichard, P. U.; Kretzschmar, R.; Kraemer, S. M., Dissolution mechanisms of goethite in the presence of siderophores and organic acids. *Geochimica et Cosmochimica Acta*. 2007. 71(23): 5635-5650.

Rodríguez, H.; Fraga, R., Phosphate solubilizing bacteria and their role in plant growth promotion. *Biotechnology Advances* 1999. 17(4–5), 319-339.

Royt, P. W., Pyoverdine-mediated iron transport. *Biol Metals*. 1990. 3:28-33.

Ryan, P.; Delhaize, E.; Jones, D., Function and mechanism of organic anion exudation from plant roots. *Annual Review of Plant Physiology and Plant Molecular Biology* 2001. 52(1): 527-560.

Santos, E. C.; Jacques, R. J. S.; Bento, F. M.; Peralba, M. C. R.; Selbach, P. A.; Sa, E. L. S.; Camargo, F. A. O., Anthracene biodegradation and surface activity by an iron-stimulated Pseudomonas sp. *Bioresource Tech.* 2007. 99:2644-2649.

Sarniguet, A.; Kraus, J.; Henkels, M. D.; Muehlchen, A. D.; Loper, J. E., The sigma factor σ^s affects antibiotic production and biological control activity of Pseudmonas fluorescens Pf-5. *PNAS*. 1995. 92:12255-12259.

Schalk, I. J., Metal trafficking via siderophores in gram-negative bacteria: specificities and characteristics of the pyoverdine pathway. *J Inorg Biochem.* 2007. 102:1159-1169.

Schleissner, C.; Reglero, A.; Luengo, J. M., Catabolism of D-glucose by Pseudomonas putida U occurs via extracellular transformation into D-gluconic acid and induction of a specific gluconate transport system. *Microbiology* 1997. 143(5): 1595-1603.

Schlesinger, W. H.; Andrews, J. A., Soil respiration and the global carbon cycle. *Biogeochemistry*. 2000. 48(1):7-20.

Shakoury-Elizeh, M.; Protchenko, O.; Berger, A.; Cox, J.; Gable, K.; Dunn, T. M.; Prinz, W. A.; Bard, M.; Philpott, C. C., Metabolic response to iron deficiency in Saccharomyces cerevisiae. *Journ. Biolog. Chem.* 2010. 285(19): 14823-14833.

Sposito, G., The chemistry of soils, 1989. In Oxford University Press, New York.

Stintzi, A.; Cornelis, P.; Hohnadel, D.; Meyer, J.-M.; Dean, C.; Poole, K.; Kourambas, S.; Krishnapillai, V., Novel pyoverdine biosynthesis gene(s) of Pseudomonas aeruginosa PAO. *Microbio*. 1996. 142: 1181-1190.

Sudarsan, S.; Dethlefsen, S.; Blank, L. M.; Siemann-Herzberg, M.; Schmid, A. The functional structure of central carbon metabolism in Pseudomas putida KT2440. *Appl Environ Microbiol*. 2014. 80(17).

Sullivan, B. W.; Kolb, T. E.; Hart, S. C.; Kaye, J. P.; Dore, S.; Montes-Helu, M. Thinning reduces soil carbon dioxide but not methane flux from southwester USA ponderosa pine forests.. *Forest Ecology and Management*. 2008. 257(4): 1373.

Trivedi, P.; Sa, T., Pseudomonas corrugata (NRRL B-30409) Mutants Increased Phosphate Solubilization, Organic Acid Production, and Plant Growth at Lower Temperatures. *Current Microbiology* 2008. 56(2): 140-144.

Van der Werf, M. J.; Overkamp, K. M.; Muilwijk, B.; Koek, M. M.; Van der Werf-van der Vat, B. J. C.; Jellema, R. H.; Coulier, L.; Kankemeier, T., Comprehensive analysis of the metabolome of Pseudomonas putida S12 grown on different carbon sources. *Mol BioSyst.* 2008. 4:315-327.

Van Duuren, J.; Puchalka, J.; Mars, A. E.; Bucker, R.; Eggink, G.; Wittmann, C.; Martins dos Santos, V. Reconciling in vivo and in silco key biological parameters of Pseudomonas putida KT2440 during growth on glucose under carbon-limited condition. *BMC Biotechnology*. 2013. 13(93).

Vemuri, G. N.; Altman, E.; Sangurdekar, D. P.; Khodursky, A. B.; Eiteman, M. A., Overflow Metabolism in Escherichia coli during Steady-State Growth: Transcriptional Regulation and Effect of the Redox Ratio. *Applied and Environmental Microbiology* 2006. 72(5): 3653-3661.

Vemuri, G. N.; Eiteman, M. A.; McEwen, J. E.; Olsson, L.; Nielsen, J., Increasing NADH oxidation reduces overflow metabolism in Saccharomyces cerevisiae. *Proceedings of the National Academy of Sciences* 2007. 104(7): 2402-2407.

Visca, P.; Imperi, F.; Lamont, I.L., Pyoverdine siderophores: from biogenesis to biosignificance. *Trends in Microbiology*. 2007. 15(1):22-30.

Vyas, P.; Gulati, A., Organic acid production in vitro and plant growth promotion in maize under controlled environment by phosphate-solubizing fluorescent Pseudomonas. *BMC Microbiol*. 2009. 9:174.

Wang, C. H.; Stern, I. J.; Gilmour, C. M., The catabolism of glucose and gluconate in Pseudomonas species. *Arch Biochem Biophys*. 1959. 81:489-492.

Weitzel, M.; Noh, K.; Dalman, T.; Niedenfuhr, S.; Stute, B.; Wiechert, W., 13CFLUX2 high performance software suit for ^{13}C-metabolic flux analysis. *Bioinformatics*. 2012. 29(1):143-145.

Wenyun, L.; Clasquin, M. F.; Melamud, E.; Amador-Noguez, D.; Caudy, A. A.; Rabinowitz, J. D., Metabolomic analysis via reversed-phase ion-pairing liquid chromatography coupled to a stand alone orbitrap mass spectrometer. *Anal Chem*. 2010. 82(8):3212-3221.

Winsor, G. L.; Lam, D. K.; Fleming, L.; Lo, R.; Whiteside, M. D.; Yu, N. Y.; Hancock, R. E.; Brinkman, F. S. Pseudomonas genome database: improved comparative analysis and population genomics capability for Pseudomonas genomes. *Nucleic Acids Res*. 2011. 39:596-600.

Wood, W. A., Schwerdt, R. F., Carbohydrate oxidation by Pseudomonas fluorescens. H. Mechanism of hexose phosphate oxidation. *J Biol Chem.* 1954. 206:625-635.

Xiao, R.; Kisaalita, W. S., Fluorescent Pseudomonad pyoverdines bind and oxidize ferrous ion. *Applied and Environmental Microbiology*. 1998. 64(4): 1472-1478.

Yeterian, E., Martin L. W.; Guillon, L.; Journet, L.; Lamont, I. L.; Schalk, I. J.,. Synthesis of the siderophores pyoverdine in Pseudomonas aeruginosa involves a periplasmic maturation. 2010. 38(5): 1447-59.

Yuan, J.; Bennett, B. D.; Rabinowitz, J., Kinetic flux profiling for quantification of cellular metabolic fluxes. *Nature Protocols*. 2008. 3(8):1328-1340.

Zamboni, N.; Fendt,S. M.; Ruhl, M.; Sauer, U., ^{13}C-based metabolic flux anaylsis. *Nature Protocols*. 2009. 4(6):878-892.